Review

Recognizing the Beauty of Myelination through Identifying Sites of Phospholipid, Protein, and RNA Syntheses and Characterizing Their Movements in Myelin Internodes

Robert Gould * and Alexander Gow

Posted Date: 10 May 2024

doi: 10.20944/preprints202405.0549.v1

Keywords: Schwann cells; oligodendrocytes; myelination; autoradiography; phosphatidylcholine; phosphatidylinositol; bio-orthogonal precursors

Review

Recognizing the Beauty of Myelination through Identifying Sites of Phospholipid, Protein, and RNA Syntheses and Characterizing Their Movements in Myelin Internodes

Robert M. Gould [1,*] and Alexander Gow [2,3,4]

[1] Whitman Research Center, Marine Biological Laboratory, 7 MBL Street, Woods Hole, MA 02543; rmgould48@gmail. com
[2] Center for Molecular Medicine and Genetics,
[3] Department of Pediatrics,
[4] Department of Neurology, Wayne State University, 3217 Scott Hall, 540 E Canfield, Detroit MI 48201; agow@med.wayne.edu
* Correspondence: rmgould48@gmail.com

Abstract: We used light, electron microscope and teased fiber autoradiography to show that myelinating Schwann cells synthesize phospholipids and proteins in perinuclear cytoplasm and superficial cytoplasmic channels or Cajal bands (SCC/CB). Neither phospholipid nor protein syntheses occur in paranodal loops, Schmidt-Lanterman incisures or adaxonal cytoplasm. Autoradiographic studies also show that in support of local protein synthesis, RNAs move from the nucleus into perinuclear cytoplasm and out along SCC/CB. Unlike other phospholipids, phosphatidylinositol synthesis occurs extensively in axons. This finding indicates differences in the distributions of phospholipid synthesizing enzymes in smooth endoplasmic reticulum of Schwann cell processes and axoplasm. Autoradiographs of nerves at longer survival times show that tritiated phosphatidylcholine and fucose-labeled glycoproteins move from synthetic sites to outermost myelin lamellae. From there, phosphatidylcholine spreads inward reaching innermost lamellae of thicker sheaths in days. Coupled with retention of fucose glycoproteins in outer myelin lamellae is the presence of fucose glycoprotein synthesized during early myelination in inner lamellae of thicker sheaths, a result consistent with growth of myelin sheaths from inner lamellae out. In this review, we revisit these studies because they provide temporal and spatial perspectives needed in understanding dynamic aspects of myelinogenesis and how myelinating cells respond to injury and from altered gene expression.

Keywords: schwann cells; oligodendrocytes; myelination; autoradiography; phosphatidylcholine; phosphatidylinositol; bio-orthogonal precursors

1. Introduction

Having studied myelination for years, we realize that current efforts that determine how molecules of interest (proteins, lipids and genes) influence myelination rely on morphological and compositional changes as readouts, readouts that will not uncover underlying spatial and temporal changes that precede and are responsible for observed changes. To move forward, we believe that it will be important to look back at Schwann cell-based myelination in terms of the spatial (identifying intracellular sites where lipids and proteins are synthesized) and temporal (recording movements of phospholipids, glycoproteins and RNAs within individual internodes) learned from autoradiographic studies. To understand these spatial and temporal features, we revisit these studies, and describe the importance of these approaches in gaining novel insights of myelin dynamics.

Examining approaches that first garnered spatial and temporal information of myelin dynamics will be our starting point. By examining rates at which myelin basic protein (MBP) and proteolipid protein (PLP1) enter myelin, it was found that MBP enters myelin far more rapidly than PLP1 [1–3].

 doi:10.20944/preprints202405.0549.v1

Follow up studies showed that the rapid MBP entry occurs because *MBP* mRNA-containing polyribosomes are located near sites of myelin assembly, determined by the selective trapping of *MBP* mRNA in myelin vesicles during tissue homogenization [2] and by differences in distributions of *MBP* mRNA (spread into processes) versus *PLP1* mRNA (restricted to soma) as obtained by *in situ* hybridization [4]. Related studies showed that similar differences occur during PNS myelination. Here too, MBP enters peripheral nerve myelin far more rapidly than myelin protein zero (MPZ) [5], results supported by differences in locations of *MBP* (spread) and *MPZ* (soma only) mRNAs as seen in *in situ* hybridization studies [6,7].

In accordance with different location of MBP (myelinating cell processes) and (PLP1/MPZ) syntheses (somata), autoradiographic studies show that following injections of tritiated amino acids into mouse sciatic nerves, proteins are synthesized in both perinuclear regions (PLP1) and in SCC/CB (MBP, [8,9]). These findings provide morphological visualization of distinct locations where syntheses of these proteins occur. Furthermore, in addition MBP, myelinating oligodendrocytes, and likely Schwann cells, contain other mRNAs that co-localize with *MBP* mRNA in processes, indicating that silver grains in SCC/CB, not only represent MBP synthesis, but other proteins important for myelination [10–12]. Taken together, these studies demonstrate spatial separations of sites where different myelin-destined proteins are synthesized, information not extracted in readouts typically used to assess myelination.

Whereas MBP, PLP1 and MPZ are unique to myelin [13,14], enabling straightforward comparisons of their rates of entry into myelin, no lipids, be it phospholipids, cholesterol or galactolipids, are unique to myelin [15–19]. Hence, approaches used to uncover differences in the entries of proteins into myelin, cannot be used for lipids. Autoradiographic studies are able to show that synthesis of all major phospholipids, including phosphatidylcholine [8,20,21], phosphatidyl-inositol [8,22], phosphatidylethanolamine and phosphatidylserine [8]) occur in perinuclear areas and SCC/CB. However, these studies are not able to show if lipids synthesized in perinuclear regions are compositionally different from lipids synthesized in SCC/CB. As yet, autoradiography has not been used to identify sites where syntheses of cholesterol, and galactocerebroside and sulfatide occur, nor movements from these sites into myelin. Studies that address these shortcomings are discussed in section 3.2.

Another approach that has not been applied to locating sites of phospholipid synthesis is immunocytochemistry. It seems reasonable to consider conducting immunocytochemistry studies to determine distributions of lipid synthetic enzymes among perinuclear regions, SCC/CB, Schmidt-Lanterman incisures, paranodal loops and adaxonal cytoplasm. Immunohistochemistry has been used to clearly show that ceramide synthase (CerS2), and, hence, ceramide synthesis, a precursor of sphingomyelin, galactocerebroside and sulfatide, is present in both perinuclear cytoplasm and in SCC/CB [23]. Interestingly, these studies did not find that CerS2 was distributed to myelinating oligodendrocyte processes. It should be possible to get more detailed information on distributions of enzymes of interest among cytoplasmic regions, by counterstaining with antibodies to proteins located in these regions. Overall, the autoradiographic findings indicate that organelles (polyribosomes, (protein), smooth endoplasmic reticulum (lipid, [24]), peroxisomes (lipid, [25,26]) and mitochondria) needed for protein and lipid [27–29]) syntheses are distributed throughout the SCC/CB to facilitate the rapid entry of nascent proteins and lipids along myelin internodes.

Here, we revisit the autoradiographic evidence that identify morphological sites of phospholipids and protein syntheses and that follow movements of phosphatidylcholine and fucosylated glycoproteins from synthetic sites into myelin. We then discuss the feasibility of expanding these studies to determine whether cholesterol, and galactolipids are similarly synthesized in perinuclear regions and SCC/CB and whether movements to and through myelin differs among lipid and protein constituents. Because studies have not identified morphological sites of lipid, protein and RNA syntheses in myelinating oligodendrocytes, nor movements into myelin (lipids and proteins) and along internodes (RNAs, we discuss the feasibility of conducting autoradiographic studies on oligodendrocyte-based CNS myelination, as well as the possibility of

 doi:10.20944/preprints202405.0549.v1

using noncanonical amino acids and bio-orthogonal precursors to other macromolecules can be used to uncover novel information on myelin dynamics.

2. What We Have Learned of Peripheral Nerve Myelination from Autoradiographic Studies

To understand how myelinating cells expand their plasma membranes to spirally wrap large caliber axons, one must know where the lipid and protein constituents of compact myelin are synthesized, how they are targeted and transported to myelin. As compact myelin is structurally and compositionally different from the myelinating cell's plasma membrane, i.e., the former is uniquely lipid-rich [30] with evolutionarily-novel proteins [14], identifying sites where myelin-constituent proteins and lipids are synthesized and how they are moved to myelin must be understood.

Although lacking in resolution needed to provide some details, autoradiographic studies clearly locate sites where syntheses of peripheral nerve myelin-destined phospholipids and proteins occurs and the time course of movements into myelin sheaths. Unfortunately, recent papers and reviews that highlight advances in understanding mechanisms of myelination either misinterpret or fail to include these findings. We believe that advancing understanding of myelin sheath assembly and maintenance needs to be built on the autoradiographic data with forward thinking approaches.

2.1. Identifying Sites Where Myelinating Schwann Cells Synthesize Phospholipids

Because it phospholipids located in myelin sheaths have extremely low turnover rates compared with phospholipids located in other brain organelles [31,32], we chose to find out if phospholipids remain permanently in myelin sheaths of mature animals, or are they replaced. To approach this question, we were attracted by autoradiography studies that visualized the accumulation of tritiated choline-labeled phospholipids in growing myelin sheaths in Schwann cells-dorsal root ganglia co-cultures [33] and that tracked the movements of tritiated fatty acid-containing lipids from endoplasmic reticulum to lipid droplets in several cell types [34–36]. Hence, we chose using an autoradiography approach to find out if tritiated choline-labeled phosphatidylcholine synthesized by myelinating Schwann cells *in vivo* in adult mice and frog nerves is incorporated into myelin sheaths [20]. We observed that shortly after intraneural injection into expoased nerves, tritiated choline incorporation into phospholipid, predominantly phosphatidylcholine, occurred predominantly in perinuclear regions of myelinating Schwann cells and not at all in myelin. Images of grain distributions representing locations of nascent phosphatidylcholine are shown in mouse sciatic nerves (Figure 1). Light microscope autoradiographs show prominent accumulations in crescent-shaped perinuclear regions (arrows, Figure 1A) and lesser accumulations along outer lamellae of compact myelin. Accumulations also occur in unmyelinated fibers (not shown), in perivascular and endoneurial cells, though not in Schwann cell nuclei, compact myelin, Schmidt-Lanterman incisures, myelinated axons or the extracellular space. We observe similar accumulation patterns in frog sciatic nerves (not shown). Electron microscope autoradiographs (Figure 1B) reinforce these findings, showing prominent nascent phosphatidylcholine accumulation in perinuclear Schwann cell cytoplasm (arrow, Figure 1B), along Schwann cell/myelin and extracellular space/myelin junctions (arrowheads, Figure 1B), though not in Schwann cell nuclei, Schmidt-Lanterman incisures, compact myelin, axons, or the extracellular space.

 doi:10.20944/preprints202405.0549.v1

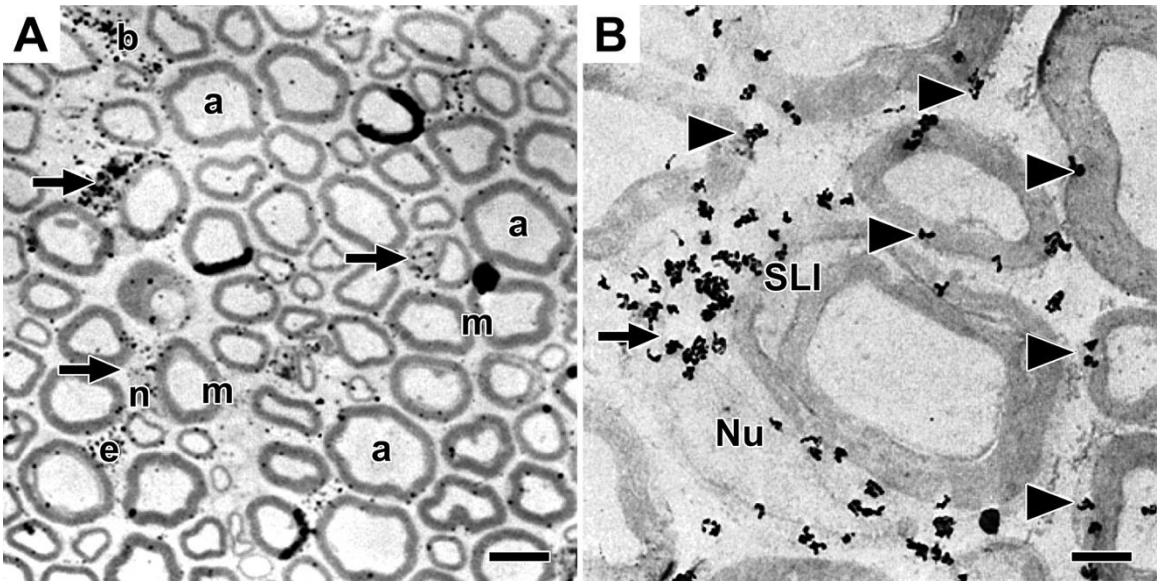

Figure 1. Distribution of tritiated choline-labeled phosphatidylcholine in mouse sciatic nerves twenty minutes after precursor injection. Legend: Silver grains represent sites of tritiated choline labeled phospholipid, mainly phosphatidylcholine. (A) In light microscope images, labeled phosphatidylcholine concentrates in perinuclear Schwann cell cytoplasm (arrows), and to some extent also in cytoplasmic pockets outside compact myelin, i.e., SCC/CB, in cells lining (b) blood vessel walls in (e) endothelial cells though not in Schwann cell nuclei (n), myelin sheaths (m) or myelinated axons (a). (B) In electron microscope images, nascent phosphatidylcholine clusters over perinuclear Schwann cell cytoplasm (arrow), along SCC/CB(arrowheads), though not over Schwann cell nuclei (Nu), Schmidt-Lanterman incisure (SLI), compact myelin or axons. Pictures are reproduced with some modifications of Figures 3A and 4A in [20] shown with permission from the publisher.

To provide a novel perspective of nascent phosphatidylcholine distributions in Schwann cell internodes, we prepared and examined autoradiographs of teased fibers fixed twenty minutes after tritated choline injection [37]. With emulsion covering teased fiber surfaces, images highlight presences of nascent phosphatidylcholine in both perinuclear regions and along regions of SCC/CB facing the emulsion (Figure 2A). Near-uniform distributions of nascent phosphatidyl-choline over SCC/CB, as seen with visual comparisons of grain densities near perinuclear regions (Figure 2B, a, b and c) versus near nodes (Figure 2B, d, arrows) suggest similar levels of local synthesis throughout these regions. Vesicular and non-vesicular transport from perinuclear regions. would be seen as pronounced proximal-distal labeling gradients.

 doi:10.20944/preprints202405.0549.v1

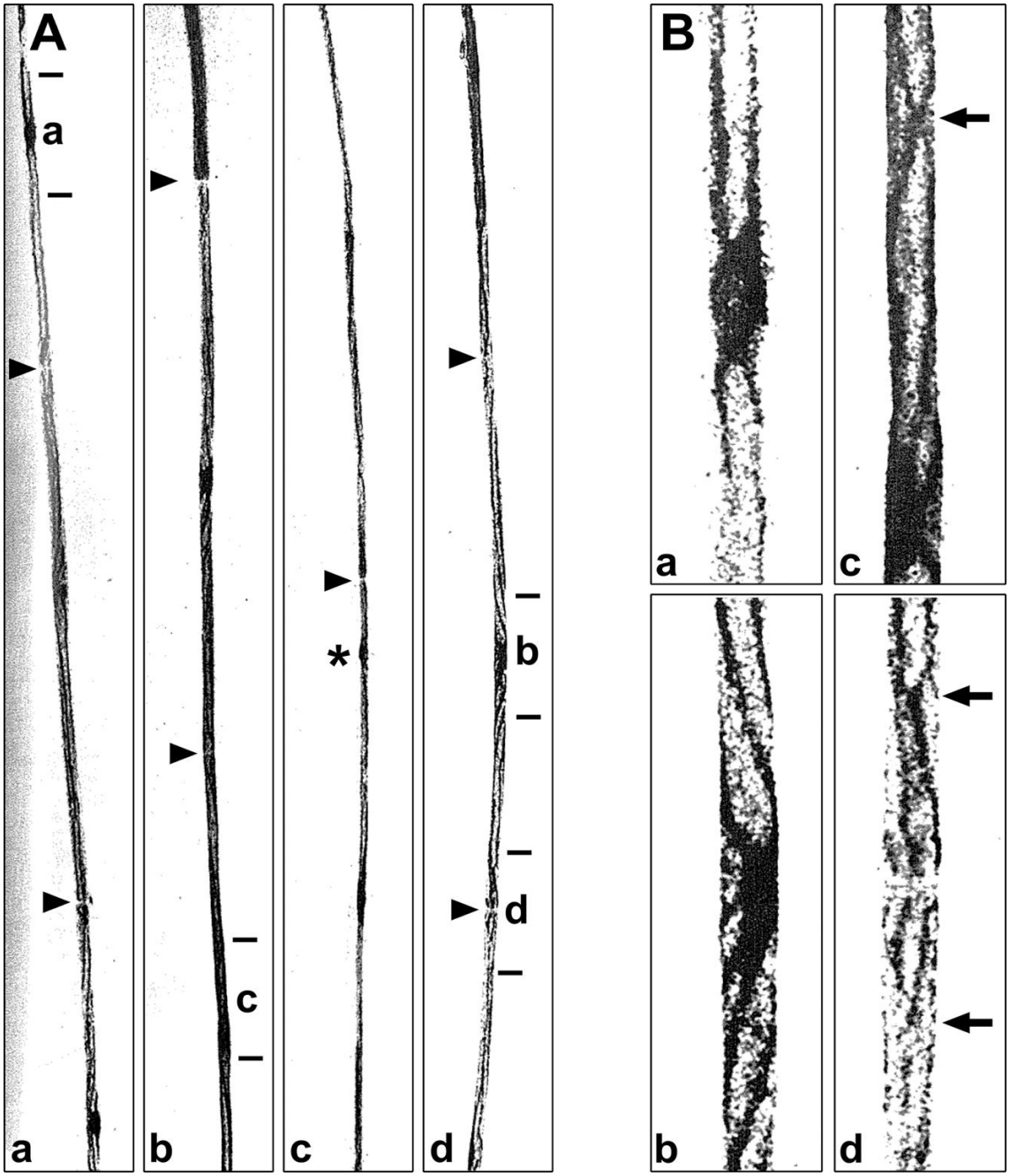

Figure 2. Teased fiber autoradiographs showing distribution of nascent phosphatidylcholine. Legend: A) Teased fibers (a, b, c and d) were prepared from mouse sciatic nerve injected with tritiated choline and fixed by drip perfusion with glutaraldehyde solution twenty minutes later. All four fibers were photographed at 136X. Arrows mark nodes of Ranvier. Asterisk marks a region along an SCC/CB with uniquely high levels of phosphatidylcholine. Letters (a, b, c and d) along fibers mark positions shown at higher magnification in B. B) Enlargements (600X) of portions of teased fibers displayed in A. a, b and c show perinuclear regions, whereas d shows labeling surrounding a node of Ranvier. Regions of branching characteristic of SCC/CB are marked with arrows (c and d). Figures 1 and 2 are reproduced from Figures 1 and 2 in [21], with permission from the publisher.

Taken together, these results indicate that cytoplasm and endoplasmic reticulum distributed throughout perinuclear regions and SCC/CB contain enzymes (choline kinase, CTP:phosphocholine-cytidyl transferase and choline phosphotransferase) that enable local phosphatidylcholine synthesis, and that these enzymes are absent or far less active in cytoplasm and endoplasmic reticulum that extend into paranodal loops, Schmidt-Lanterman incisures and adaxonal regions.

 doi:10.20944/preprints202405.0549.v1

To find out if other phospholipids are similarly synthesized in perinuclear regions and SCC/CB, we compared distributions of phospholipids in nerves labeled with tritiated choline, with distributions in nerves labeled with tritiated glycerol, ethanolamine, and serine at the same two-hour time (Figure 3). Distribution patterns of phosphatidylcholine (Figure 3A) are unchanged from patterns at twenty minutes (Figure 1), i.e., high expression in perinuclear regions (arrow and C, Figure 3A), along SCC/CB (arrowheads, Figure 3A), including paranodes (P, Figure 3A). Phospholipids synthesized from tritiated glycerol (Figure 3B), a mix of phosphatidylcholine, phosphatidylethanolamine, phosphatidylserine and phosphatidylinositol [38]; tritiated ethanolamine (Figure 3C), a mix of phosphatidylethanolamine and ethanolamine plasmalogen [38]), and tritiated serine (Figure 3D), mostly phosphatidylserine [38]; are distributed similarly to one another and to that of nascent phosphatidylcholine. All nascent phospholipids concentrate in crescent-shaped perinuclear regions (arrows, Figures 3B, 3C and 3D) and along SCC/CB (arrowheads, Figures 3B, 3C and 3D). None accumulate in Schmidt-Lanterman incisures (S, Figures 3B, 3C and 3D), myelin sheaths, axons, or the extracellular space. Hence, all major phospholipids are synthesized in myelinating Schwann cell perinuclear regions and along SCC/CB.

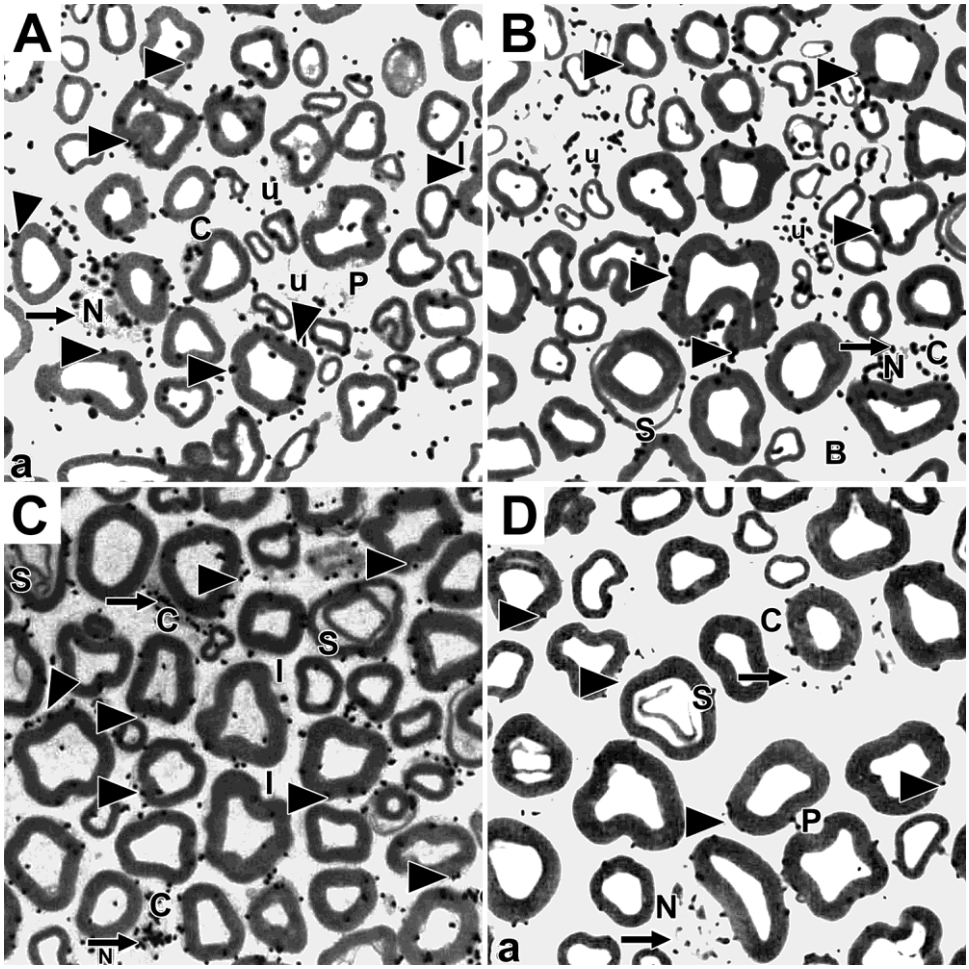

Figure 3. Sites of tritiated choline, glycerol, ethanolamine and serine incorporation into phospholipids two hours after precursor injections into mouse sciatic nerves. Legend: Light microscopic autoradiographs of mouse sciatic nerves in cross section. Nerves were injected with tritiated: A) choline, B) glycerol, C) ethanolamine and D) serine and fixed after two hours. As in previous figures, arrows mark perinuclear regions and arrowheads point to silver grains at Schwann cell/myelin and extracellular space/myelin interfaces. Abbreviations from original publication are – C, perinuclear Schwann cell cytoplasm; N, Schwann cell nuclei; I, internodal Schwann cell cytoplasm; P, paranodal regions; S, Schmidt-Lanterman incisures; u, unmyelinated fibers; B, blood vessel. All figures are reproduced with some modifications from Figures 2A, 2B, 2C and 3A in [8] with permission from the publisher.

 doi:10.20944/preprints202405.0549.v1

Unlike other phospholipid precursors, tritiated myo-inositol is rapidly (within thirty minutes) and selectively incorporated into lipids, mainly phosphatidylinositol, in myelinated axons and unmyelinated fibers (Figures 4A and B) [8,22]. Low initial incorporation into Schwann cell perinuclear regions may be due to high endogenous myo-inositol levels in these cells [39]. At two hours, nascent phosphatidylinositol levels remain high in axons and increase Schwann cell perinuclear regions (arrows, Figure 4C). At eight hours levels in myelinating Schwann cells remain high, while levels in myelinated axons fall (Figure 4D). Clearly, these studies identify a path whereby tritiated myo-inositol, injected into perineural space, bypasses Schwann cell cytoplasm, gains rapid access to axoplasm and is incorporated into phosphatidylinositol. This result suggests that axoplasmic smooth endoplasmic reticulum is enriched in phosphatidylinositol synthase.

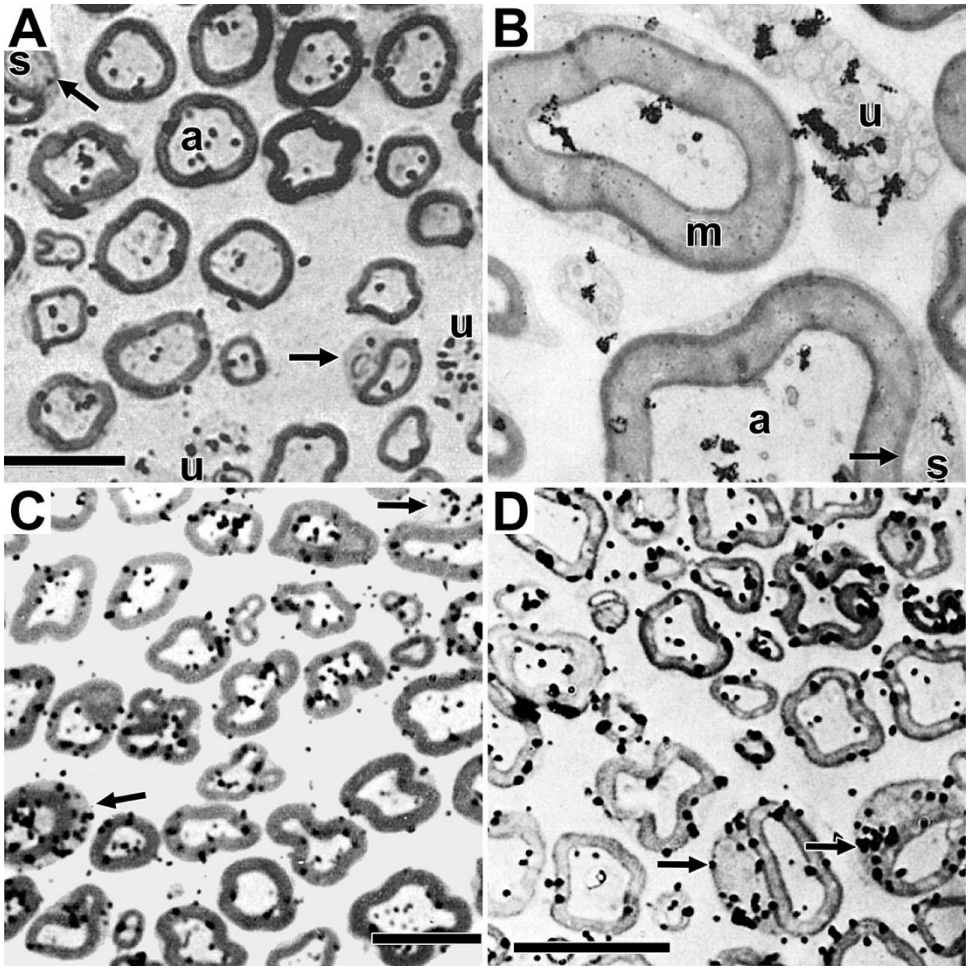

Figure 4. Distributions of tritiated myo-inositol-labeled phosphatidylinositol in mouse sciatic nerves at various times after precursor injection. Legend: Light (A, C and D) and electron microscope (B) autoradiographs of cross sections of mouse sciatic nerves fixed at thirty minutes (A and B), two hours (C) and eight hours (D) after injection of tritiated myo-inositol into sciatic nerves. Arrows point to perinuclear Schwann cell cytoplasm. Abbreviations are from original publication and are the same as in Figures 1 and 3. Figures 4A, 4B, 4C and 4D are reproduced with some modifications from Figures 1A, 1C, 1D and 1E in [22] with permission from the publisher.

For phosphatidylinositol synthase to be enriched in axoplasm, it must undergo axonal transport. Using a nerve ligation paradigm [40], we showed that phosphatidylinositol synthase selectively (compared with phosphatidylcholine synthase) accumulates proximal to a ligature by enzyme assay buildup of tritiated phosphatidylinositol in enlarged axons at the ligation site [8,20]. As further evidence that axoplasm contain phosphatidylinositol synthase, we examined lipid synthesis using axoplasm extruded from squid giant axons. Squid axoplasm had already been shown to incorporate ^{32}P-inorganic phosphate into phosphatidylinositol, phosphatidylethanolamine and phosphatidic acid

 doi:10.20944/preprints202405.0549.v1

[41]. We found that extruded squid axoplasm readily incorporates tritiated myo-inositol into phosphatidylinositol [42] and that it contains phosphatidylinositol synthase, and phosphatidylinositol kinase, diglyceride kinase and phosphatidylinositol exchange protein as measured by enzyme assay [43]. Because both rodent (mammal) and mollusk (squid) axoplasm contains phosphatidylinositol synthase and from studies with squid axoplasm, other enzymes involved in inositide metabolism, inositides likely plays evolutionarily conserved roles in axon functions.

2.2. Identifying Sites Where Myelinating Schwann Cells Synthesize Proteins and Glycoproteins

The ability of autoradiographic studies to identify morphological sites where myelinating Schwann cells synthesize phosphatidylcholine [20], led us to undertake follow up studies to identify sites where tritiated fucose, a glycoprotein-specific precursor [44], is incorporated into glycoproteins [45] and where tritiated amino acids, methionine and proline, are incorporated into protein [8,9]. One hour after tritiated fucose injection into mouse sciatic nerves, fucose-labeled glycoproteins are found to accumulate over limited portions of perinuclear Schwann cell cytoplasm (arrows, Figure 5A), regions identified as the Golgi apparatus in electron micrographs (Figures 5B and 5C). Using teased fibers, we find fucose-labeled glycoprotein distributes along SCC/CB at times ranging from twenty minutes to three hours [46], suggesting that with long exposures, it is possible to capture fucose glycoproteins undergoing rapid transport along SCC/CB, presumably at rates of those measured for axonal transport (~300 mm/day [47]).

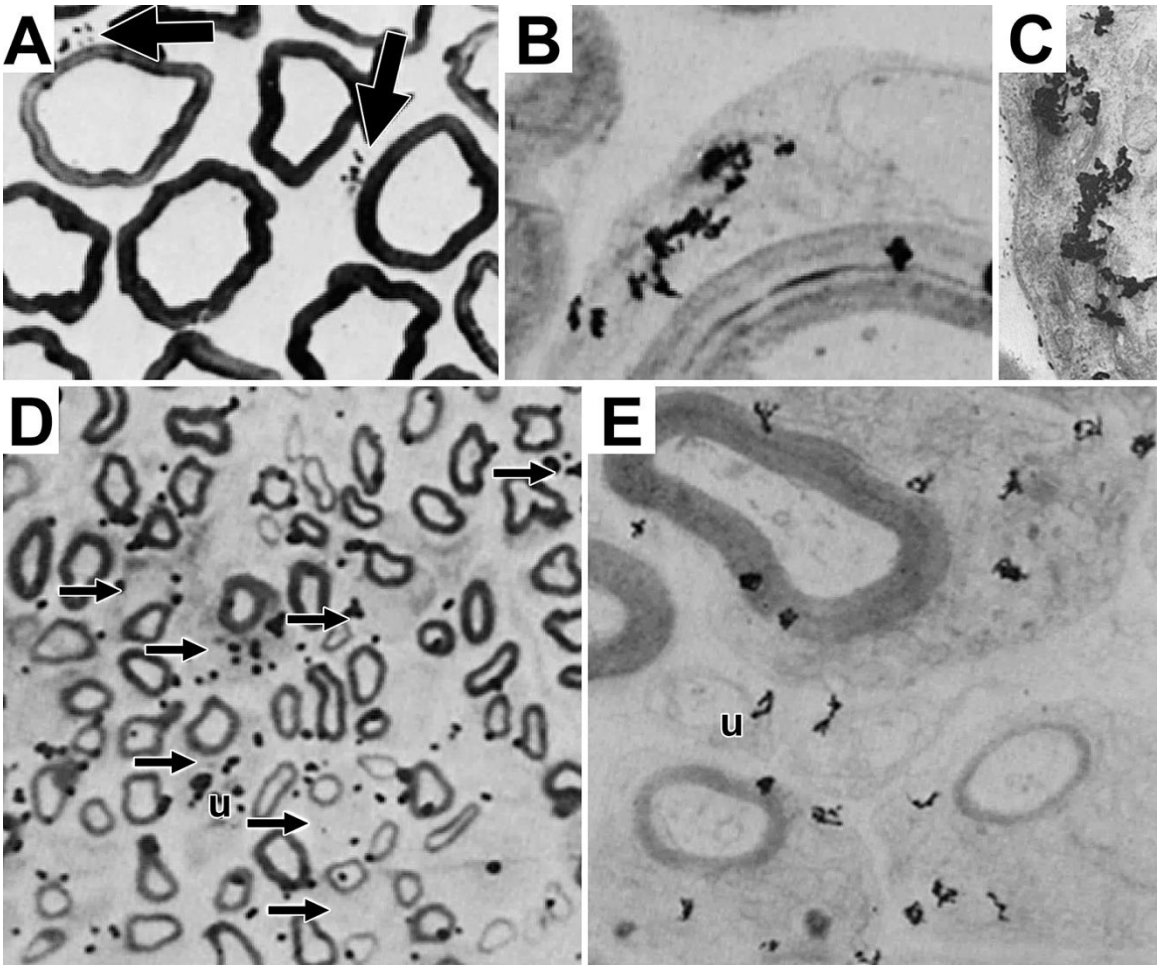

Figure 5. Distributions of tritiated fucose-labeled glycoproteins in mouse and developing rat sciatic nerves. Legend: (A) Light and (B, C) electron microscope autoradiographs showing sites of tritiated fucose incorporation into glycoproteins in adult six-month-old mouse nerves. (D) Light and (E) electron microscope autoradiographs of fucose-glycoproteins in eight-day-old rat sciatic nerves.

 doi:10.20944/preprints202405.0549.v1

Mouse nerves are fixed one hour post-tritiated fucose injection and rat nerves are fixed two hours post injection. Arrows point to myelinating Schwann cell perinuclear regions. Figures are reproduced with some modifications from Figure 2 in [45] with permission from the publisher.

We also find that protein fucosylation in eight-day-old rat sciatic nerves occurs prominently in perinuclear regions in both light (arrows, Figure 6D) and electron microscope (Figure 6E) images.

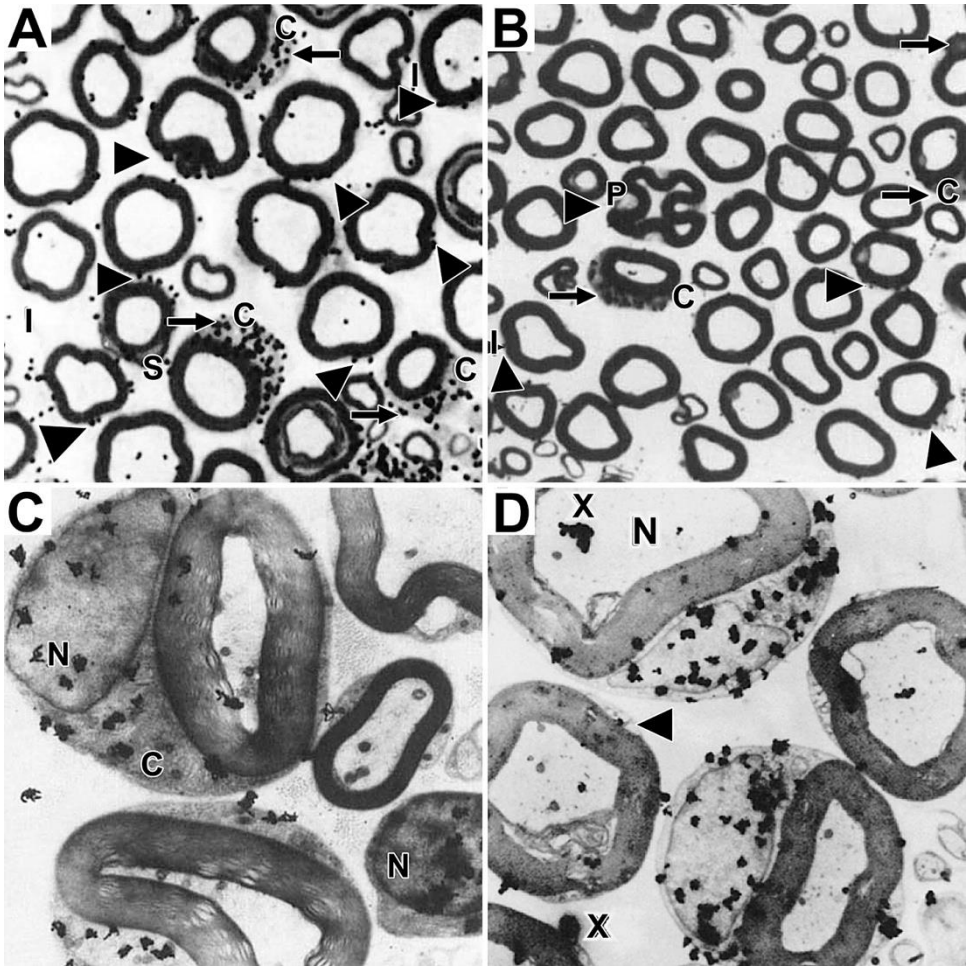

Figure 6. Distributions of tritiated methionine- and tritiated proline-labeled proteins in mouse sciatic nerves. Legend: Light (A and B) and electron microscope (C and D) autoradiographs showing sites of tritiated methionine (A and C) and tritiated proline (B and D) incorporation into proteins in six-month mouse sciatic nerves fixed two hours after precursor injection. Arrows to perinuclear regions, whereas arrowheads point to SCC/CB. Abbreviations are from the original publication, c, perinuclear Schwann cell cytoplasm; S, Schmidt-Lanterman incisure; P, paranodal area; I, internodal Schwann cell cytoplasm; N, Schwann cell nucleus and fibers with a nucleus; X, precipitates. Figures 6A - 6C were reproduced with slight modifications from [8] with permission from the publisher and Figure 6D was reproduced with slight modifications from [9] with permission from the publisher.

We identify sites of incorporation into proteins following injections of tritiated amino acids (methionine and proline) into sciatic nerves of adult mice [8,9]. Just like phospholipids (Figures 1 and 3) and glycoproteins (Figure 5), tritiated methionine and proline) are incorporated into protein predominantly in crescent-shaped perinuclear regions (arrows, Figures 6A and 6B and in SCC/CB (arrowheads, Figures 6A and 6B). Unlike phospholipids, protein synthesis is seen in Schwann cell nuclei (N, Figures 6C and 6D). Like phospholipids and glycoproteins, proteins are not synthesized in myelin sheaths, axons, Schmidt-Lanterman incisures or in the extracellular space.

 doi:10.20944/preprints202405.0549.v1

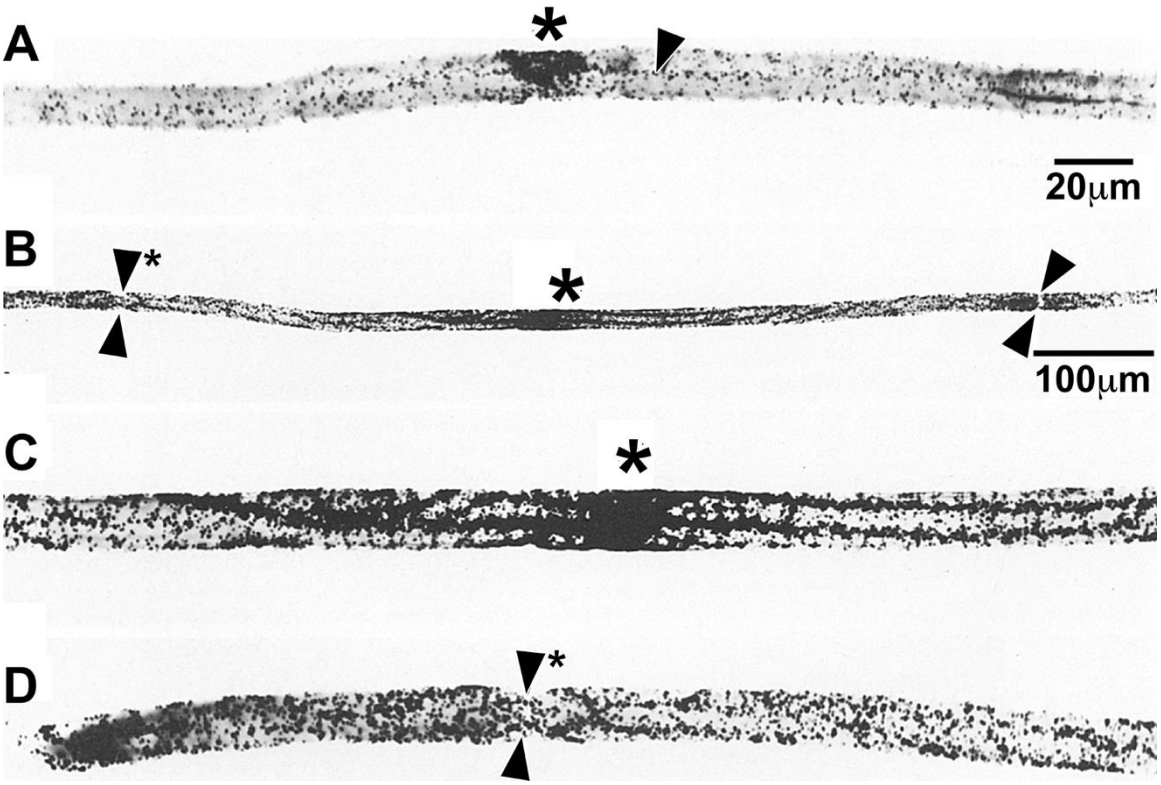

Figure 7. Teased fiber autoradiographs showing temporal distributions of tritiated proline-labeled protein in mouse sciatic nerves. Legend: Autoradiographs of adult mouse sciatic nerves labeled for one hour with tritiated proline. Fibers were exposed to emulsion for both short (A) and longer (B-D) time periods. (A) At shorter exposures, labeled protein is highly concentrated in the centrally positioned nucleus/perinuclear region (*). (B, D) At longer exposures, strong accumulations are seen in SCC/CB. Apposed arrowheads mark nodes of Ranvier. Small asterisk pointe to the node enlarged in D. Larger asterisk in B marks the perinuclear region enlarged in C. The figure is reproduced with slight modification from Figure 3 in [45], with permission from the publisher.

To obtain another perspective, we examined nascent protein distributions in teased fibers [9]. At one hour, followed by a relatively short exposure to emulsion, nascent protein is highly concentrated in nucleus/perinuclear regions (*, Figure 7A). Some nascent protein is seen emanating from the nucleus/perinuclear region (single arrowhead, Figure 7A). At longer exposures, besides labeled protein accumulation in the nuclear/perinuclear region (*, Figure 7B), prominent levels of protein are seen throughout the SCC/CB from node to node (apposed arrowheads, Figure 7B). Compared with nascent phosphatidylcholine accumulation in teased fibers (Figure 2), these results suggest that portions of lipid synthesized in SCC/CB are higher than portions of protein. Higher magnification images near the nucleus/perinuclear region (*, Figure 7C) and near a node of Ranvier (apposed arrowheads, Figure 7D) may suggest a shallow proximo-distal gradient, i.e., some transport from perinuclear region in addition to local synthesis in SCC/CB. It should be possible to determine labeling gradients with grain density scans along a number of labeled teased fibers.

To get a clearer view as to whether protein synthesis occurs in Schmidt-Lanterman incisures, paranodal loops and/or along adaxonal Schwann cell cytoplasm, we examined proline-labeled protein patterns in longitudinal sections (Figure 8). In light microscope autoradiographs, nascent protein occur accumulates prominently in nucleus/perinuclear regions (Nu, Figure 8A) and along SCC/CB (arrowheads, Figure 8A). Labeling does not occur at a node of Ranvier (double arrowhead, Figure 8A), at four Schmidt-Lanterman incisures (S, Figure 8A), in compact myelin, axons and the extracellular space. Electron microscope autoradiographs reinforce these findings (Figures 8B and 8C). They also show high levels of nascent protein over perinuclear cytoplasm (upper right, Figure 8B), in SCC/CB (fiber above Nu, Figure 8B), and in Schwann cell nuclei (Nu, Figure 8B). Little, if any, label is seen in Schmidt-Lanterman incisures (S, Figure 8B), compact myelin, axoplasm and the

 doi:10.20944/preprints202405.0549.v1

extracellular space. Similarly, compared with high levels of nascent protein along an SCC/CB, there is little, if any labeled protein at or around the node of Ranvier (double arrowheads, Figure 8C), along inner surface of compact myelin or over axoplasm. Taken together, transverse sections (Figure 6), teased fibers (Figure 7) and longitudinal sections (Figure 8) all show that, like phospholipid synthesis, protein synthesis by myelinating Schwann cells, is dominant in perinuclear regions, occurs along SCC/CB, but not in compact myelin, Schmidt-Lanterman incisures, paranodal loops, Schwann cell microvilli, adaxonal cytoplasm, axons or extracellular regions surrounding myelinated fibers.

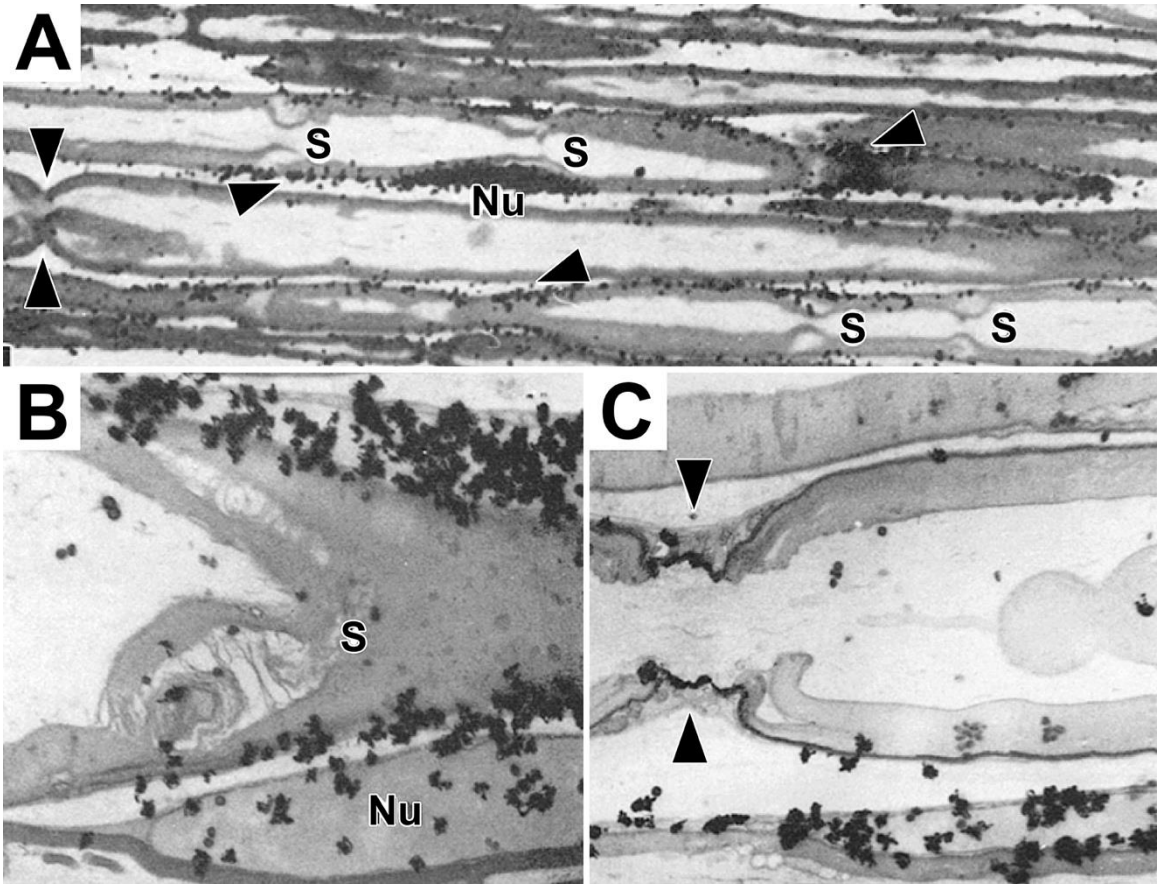

Figure 8. Distributions of newly-formed protein as seen in autoradiographs of longitudinal sections at light and electron microscope levels. Legend: Distributions of tritiated proline-labeled protein in mouse sciatic nerve at a thirty-minute labeling period. A) Light microscopy with single arrowheads pointing to labeling along SCC/CB and apposed arrowheads pointing out an unlabeled node of Ranvier. A single highly labeled Schwann cell nucleus/perinuclear region (Nu) and four unlabeled Schmidt-Lanterman incisures (S) are marked. B) Electron micrograph showing high labeling in perinuclear Schwann cell cytoplasm and in a nucleus (Nu) contrasted with limited labeling of a Schmidt-Lanterman incisure (S). C) Node of Ranvier with arrowhead pointing to lack of labeling in Schwann cell microvilli. The fiber running below the node has heavily labeled Schwann cell cytoplasm. Figure is reproduced with modification from Figures 4b, 4c and 4d in [9] with permission from the publisher.

2.3. Synthesis and Transport of RNAs by Myelinating Schwann Cells

To enable protein synthesis in the SCC/CB, protein synthetic machinery, i.e., ribosomes, tRNAs, mRNAs and many proteins involved in translation must be present. To show that RNAs access SCC/CB, we examined labeled RNA temporal changes (one hour to one week) after injecting tritiated uridine into mouse sciatic nerves [9]. At one hour, virtually all nascent RNA is in nuclei of myelinating (fiber at upper right, Figure 9A) and non-myelinating (U, Figure 9A) Schwann cells. Nearby perinuclear regions and more distant SCC/CB (arrows, Figure 9A), and unmyelinated fiber bundles lacking nuclei are unlabeled. Myelin sheaths, axons, and the extracellular space are

 doi:10.20944/preprints202405.0549.v1

unlabeled as well. The reason form two silver grains are seen over non-perinuclear cytoplasm (arrowhead, Figure 9A) is unclear. We cannot rule out artifacts of preparation.

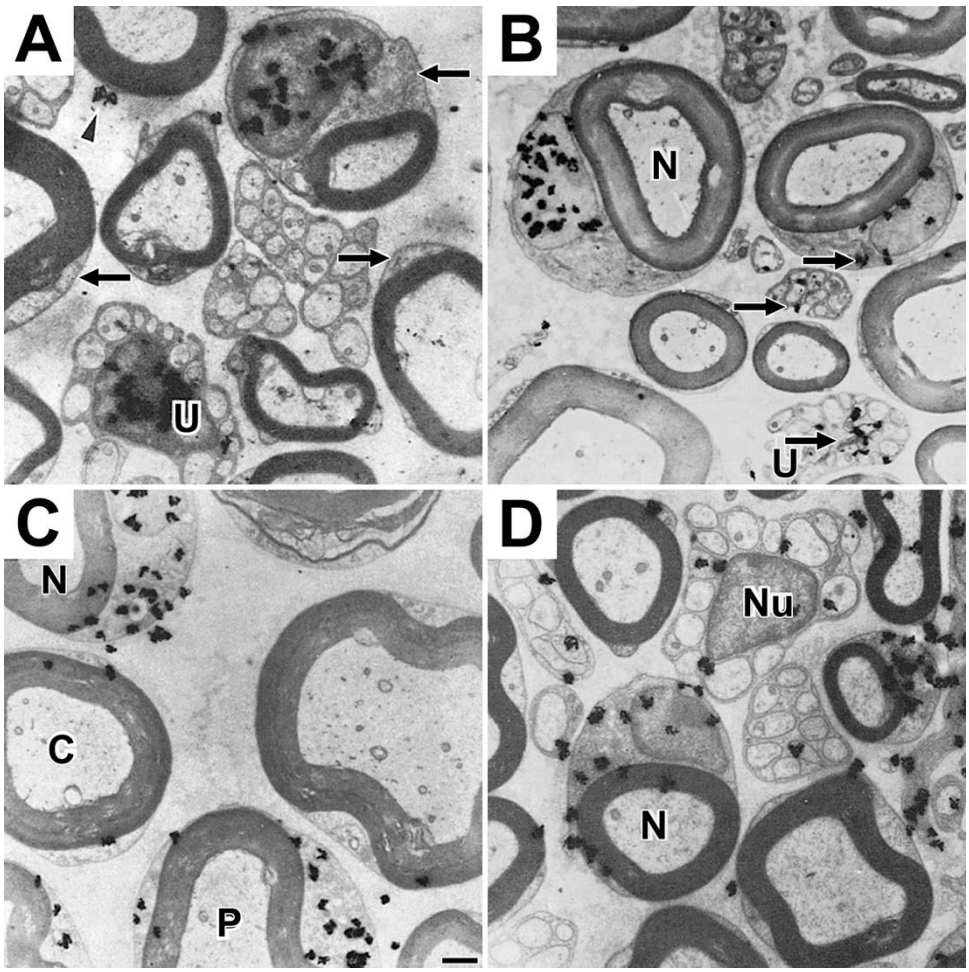

Figure 9. Electron microscopic autoradiographs showing temporal changes in distributions of tritiated uridine-labeled RNA in mouse sciatic nerves. Legend: Distributions of labeled RNA at (A) one and (B) four hours, and (C) one and (D) three days following tritiated uridine injection. Arrows point to perinuclear Schwann cell cytoplasm. Abbreviations are from original figures. Figures are reproduced with modifications from Figures 2A, 6A, 6B and 6C in [9] with permission from the publisher.

At four hours (Figure 9B), distribution patterns remain like patterns at one hour with most labeled RNA retained in Schwann cell nuclei. A few silver grains overlie perinuclear cytoplasm and unmyelinated fibers lacking nuclei (arrows, Figure 9B). At one day, large numbers of silver grains are over perinuclear cytoplasm (e.g., profiles N and P, Figure 9C) with silver grains over some SCC/CB profiles (profile C, Figure 9C). By three days, litle labeled RNA remains in myelinating and non-myelinating Schwann cell nuclei (N and Nu, respectively, Figure 9D). Now with accumulations are over perinuclear cytoplasm, SCC/CB and unmyelinated fibers.

Teased fiber autoradiographs were used to follow movements of labeled RNA into and along myelin internodes (Figure 10). At one hour, almost all labeled RNA accumulated over the Schwann cell nucleus at the internode's center (*, Figure 10A). At four hours, most labeled RNA remained in the nuclear region (*, Figure 10B), with possible spread to nearby perinuclear cytoplasm (arrowhead, Figure 10B). At one day, labeled RNA is present in SCC/CB, reaching distances roughly equal to the length of the nucleus/perinuclear region (arrowheads, Figure 10C). At three days, labeled RNA is spread further, reaching distances halfway to nodes of Ranvier (Figure 10D) and at seven days labeled RNA has spread all the way to the nodes (double arrowheads, Figure 10E). Levels of labeled RNA in regions near the perinuclear region (*, Figure 10F) are like levels at the nodes (double

 doi:10.20944/preprints202405.0549.v1

arrowhead, Figure 10G). Based on time and distances, rates (50-100 μm/day) in this *in vivo* paradigm, are comparable to rates of *MBP* mRNA transport in cultured oligodendrocytes [48] and of uridine-labeled RNA transport in neuronal dendrites [49]. Absence of amino acid-labeled protein in paranodal loops (Figure 8) make it unlikely that labeled RNA enters these structures.

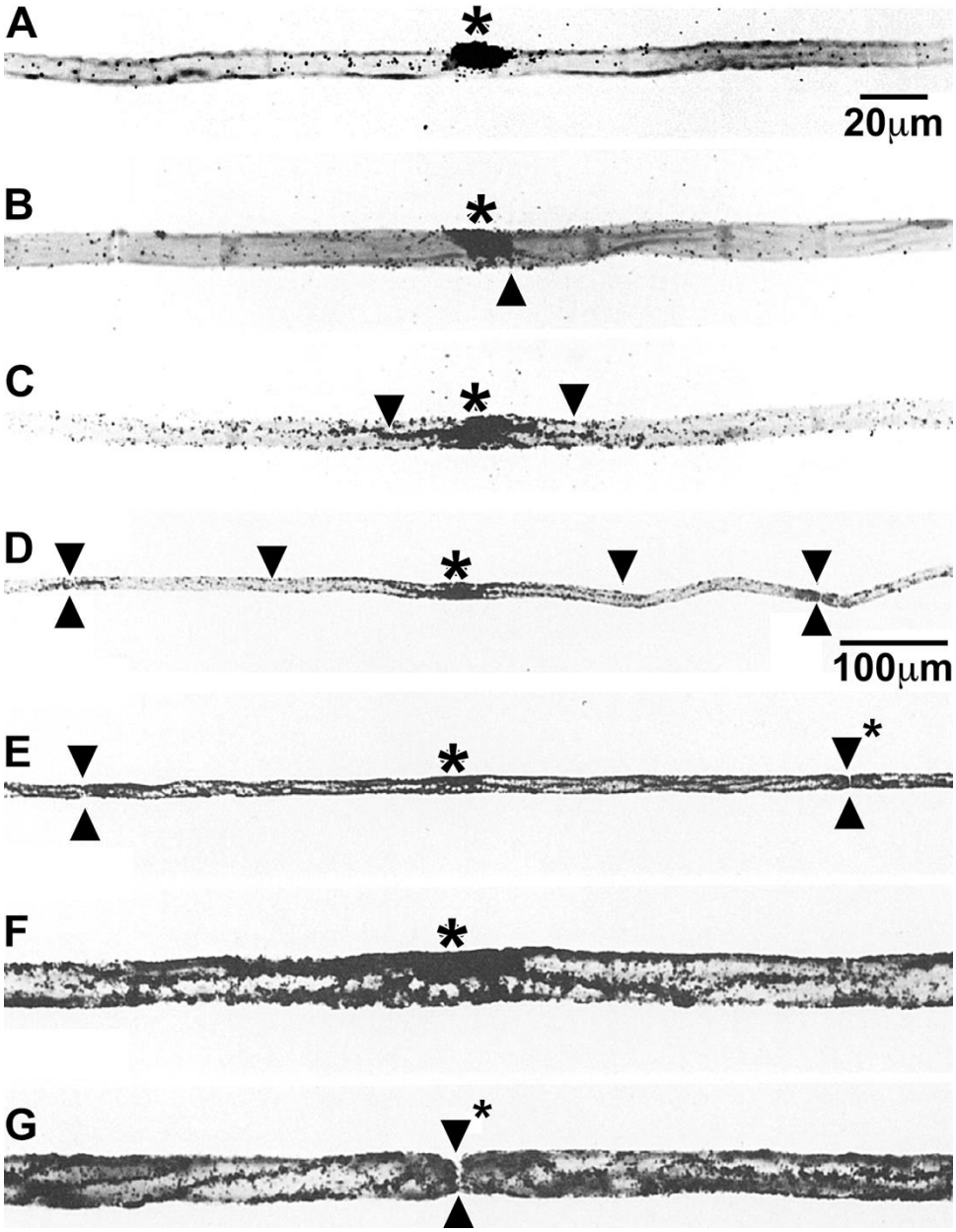

Figure 10. Teased fiber autoradiographs showing temporal changes in distributions of tritiated uridine-labeled RNA. Legend: Distribution of tritiated uridine-labeled RNA in individual teased fibers fixed at (A) one hour and (B) four hours, and (C) one, (D) three and (E) seven days. Figures F and G are enlargements of portions of Figure E. Asterisks (A – F) mark centrally-located nucleus/perinuclear area. Single arrowheads (B – F) point to front of labeled RNA in SCC/CB. Apposed double arrowheads (D, E and G) mark nodes of Ranvier. F and G are enlargements or perinuclear and paranodal areas, respectively. Figures are reproduced from Figure 5 in [9] with permission from the publisher.

2.4. Movements of Phosphatidylcholine into Myelin Sheaths

The original goal of developing an autoradiographic approach was to find out if lipids entered mature myelin sheaths [20]. Allowing animals to survive for long time periods (up to thirty-five days) following tritiated choline injection, allowed us to visualize movements into myelin. By thirty-five

 doi:10.20944/preprints202405.0549.v1

days, was almost entirely over compact myelin (Figures 11A and 11B) and no longer over perinuclear Schwann cell cytoplasm (arrows, Figure 11A).

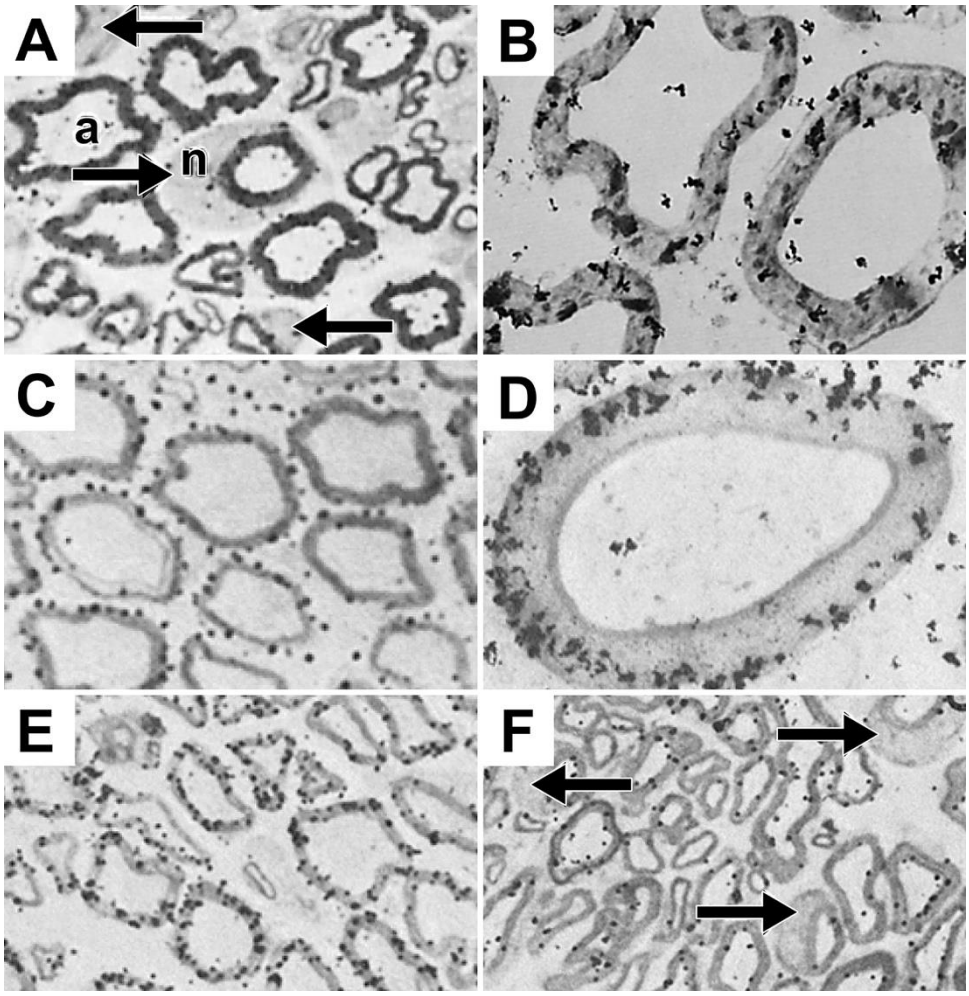

Figure 11. Distribution of labeled phosphatidylcholine and fucose glycoprotein at long survival periods. Legend: Light (A) and electron microscope (B) autoradiographs of labeled phosphatidylcholine thirty-five days after tritiated choline injection into mouse sciatic nerves. Little label is retained in perinuclear regions (arrows, A). Light (C, E and F) and electron microscope (D) images of tritiated-fucose glycoprotein in mouse sciatic nerves fixed at (C) eight, (D) eighteen and (E) seventy-two days after precursor injection and rat sciatic nerve fixed thirty-five days (F) after precursor injection into eight-day rat pup. Little label is retained in perinuclear regions (arrows, F). Figures A and B are reproduced with slight modifications from Figures 5D and 5E in [20], and Figures C, D, E and F are reproduced with slight modifications from Figures 3B, C, D and E in [45].

To determine how quickly labeled phosphatidylcholine penetrates thicker myelin sheaths, we quantified distribution patterns [50,51] at various times after precursor injections in both mouse and frog sciatic nerves. We determined silver grain densities over morphologically-distinct structures, Schwann cell cytoplasm, myelin sheaths, axons, unmyelinated fibers and the extracellular space (Table V, [20]), over junctions between them and across lamellae of thicker sheaths (Table VI, [20]). Here we plot the density distributions of mostly labeled phosphatidylcholine (>80% of total lipid [20]) over Schwann cell cytoplasm, myelin sheaths and axons (diagram on left, Figure 12A).

 doi:10.20944/preprints202405.0549.v1

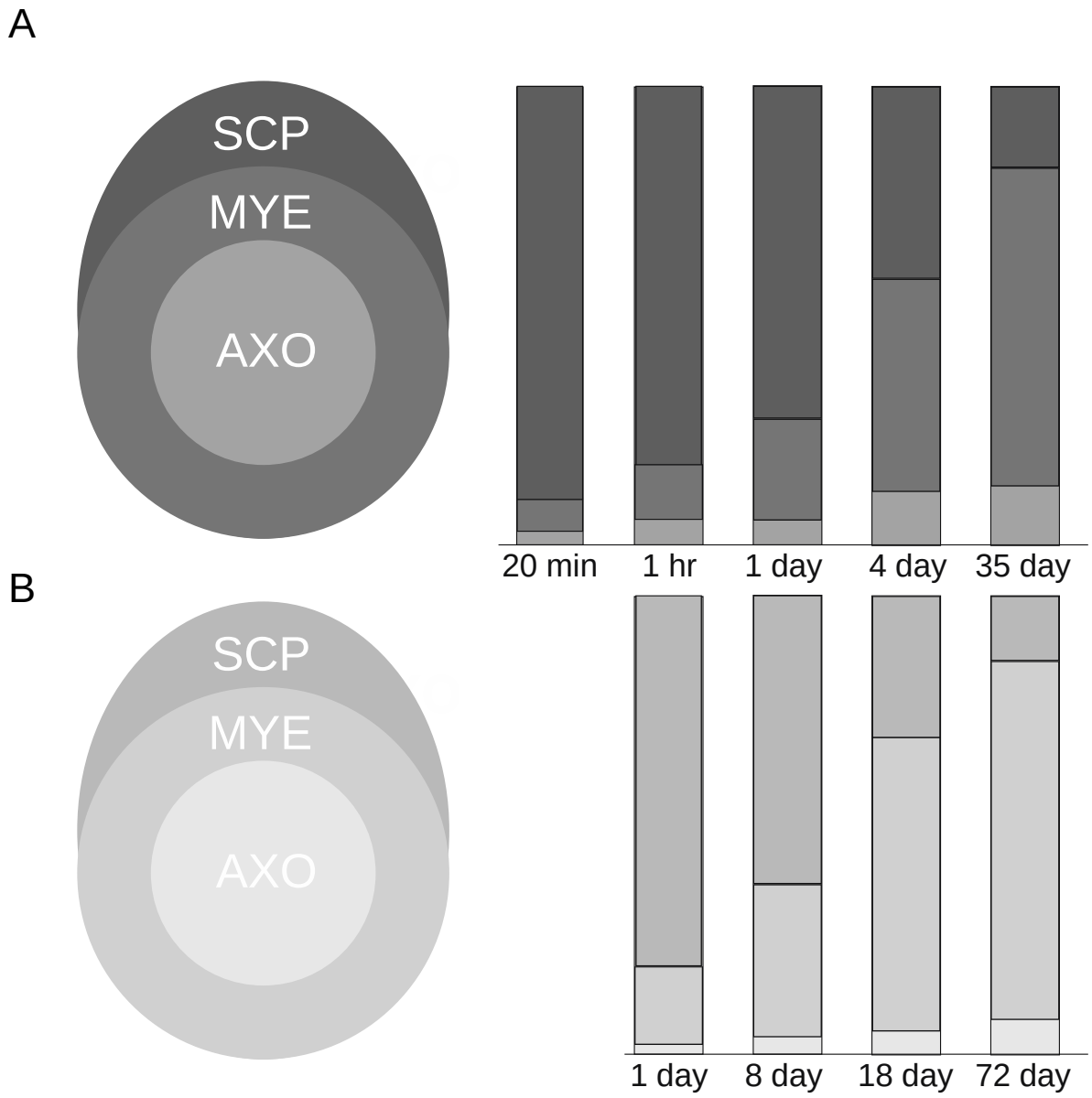

Figure 12. Temporal changes in the distributions of choline-labeled phosphatidylcholine and fucose-labeled glycoprotein among Schwann cell cytoplasm, myelin sheaths and axons in mouse sciatic nerves. Legend: Quantitative analyses showing changes in the distributions of (A) choline-labeled phospholipid and (B) fucose-labeled protein among Schwann cell perinuclear regions (SCP), myelin sheaths (MYE) and axons (AXO) at times indicated. Data for choline lipids is from Table V in [20] and for fucose-glycoprotein from Table I in [45].

As seen in nerves fixed at 20 minutes (Figure 1) and two hours (Figure 3A) post tritiated choline injection, most silver grains (>85%) are over Schwann cell cytoplasm. At one, four and thirty-five days, levels of labeled Schwann cell phosphatidylcholine fall and levels over myelin rise (Figure 12A). Levels in axoplasm remain low. In frog nerves, measurement were made at four, eight and fifteen days after tritiated choline injection [20]. Movements from Schwann cell cytoplasm to myelin occurred, but at slower rates than in mouse nerve myelin (not shown). These data capture movements of nascent phosphatidylcholine from synthetic sites in Schwann cell cytoplasm to myelin.

We examined movements of labeled choline lipids across thicker myelin sheaths [20]. In mouse nerves labeled for twenty minutes, one and four hours, myelin-associated silver grains are mostly over the two outer layers (roughly the outer third of compact lamellae. At one and four days, grain densities over these layers fall and rise in inner layers, reaching near equilibrium. By thirty-five days,

 doi:10.20944/preprints202405.0549.v1

levels remain relatively constant in all but the outermost layers, where there appears to be some fall-off. This decline in the outer layers may suggest more rapid equilibrium with unlabeled choline lipid added at the outside.

We made the same measurements across thick frog myelin sheaths at three different times [20]. At four days, labeled phosphatidylcholine was distributed similar to twenty minutes to four hour labeling of mouse nerves. Inward movements are captured at eight and fifteen days, with equilibrium reached at some time between eight and fifteen days, i.e., much slower than in mouse nerves.

2.5. Movements of Fucose-Labeled Glycoproteins into Myelin Sheaths

Temporal movements of fucose-labeled glycoprotein from Schwann cell cytoplasm to myelin were quantified (Tables I and II [45]). Plots showed that at 0ne day, most (>80%) of labeled glycoprotein was in Schwann cell cytoplasm (Figure 12B). Over a seventy-two-day time-period, movements into myelin continued to occur. Levels in myelin were greater than levels in Schwann cell cytoplasm at eighteen and seventy-two days. This movement was far slower than movements of phosphatidylcholine into mouse and frog sciatic nerve myelin (Figure 12A). Little fucose glycoprotein reached and/or was retained in axons. We also examined inward movements of fucose-glycoprotein across layers of thick mouse nerve myelin sheaths (Figure 13B). Compared with choline lipids, which had equilibrated across all layers between one and four days (Figure 13A), fucose glycoproteins remained in two outermost layers at one and eight days. At eighteen and seventy-two days, movement inward were captured. Even at seventy-two days, levels were higher in outer versus inner layers.

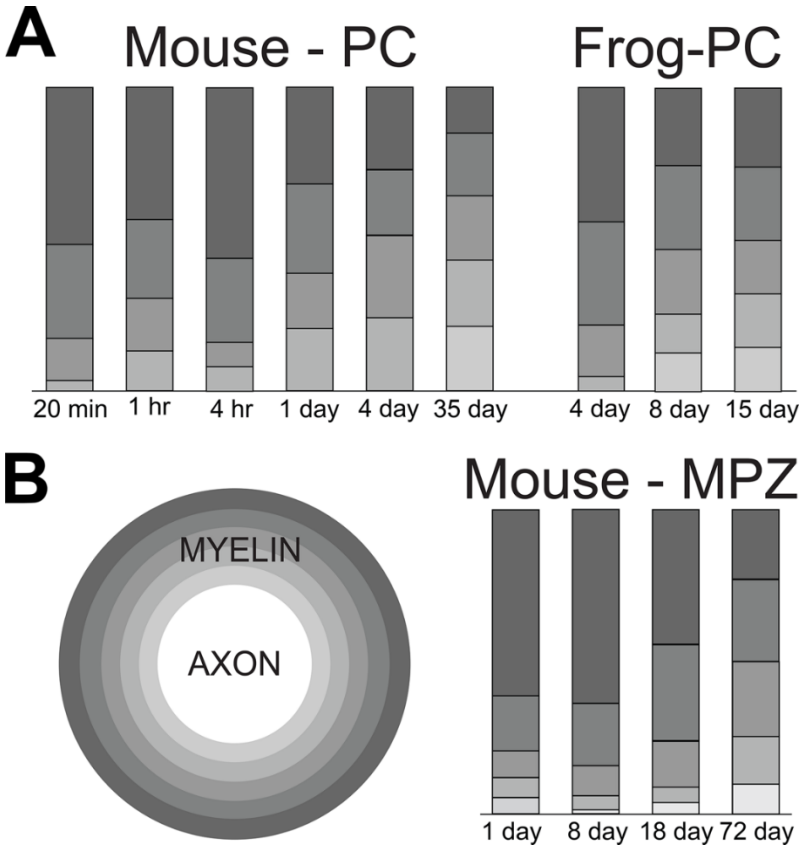

Figure 13. Temporal changes in distributions of phosphatidylcholine and fucose-glycoprotein across compact myelin. Legend: Quantitative analyses showing temporal changes in the distributions of (A) choline-labeled phosphatidylcholine (PC) over myelin layers in mouse and frog sciatic nerve sheaths and (B) fucose-labeled glycoproteins, mainly myelin protein zero (MPZ) over myelin layers in mouse sciatic nerve sheaths.

 doi:10.20944/preprints202405.0549.v1

3. Proposed Follow-up Studies

Missing from current 'myelin' research are approaches that identify sites where myelin-destined lipids and proteins are synthesized, and the paths taken to enter myelin sheaths. As demonstrated in the previous section, autoradiographic studies provide information on sites where myelinating Schwann cells synthesize phospholipids and proteins. We believe that these studies lay a foundation for future studies. We consider three ways to move forward from these studies: 3.1. Continue autoradiographic studies to further characterize peripheral nerve myelination, 3.2. Expand autoradiographic studies to CNS myelination, (3.3), conduct alternative non-autoradiographic studies to provide complementary information showing sites of lipid and protein synthesis in myelinated PNS and CNS tissues and in *in vitro* myelinating models and characterize movements from synthetic sites to myelin and non-myelin internodal sites (3.4). With these approaches, it should be possible to augment studies to better understand how injury, disease and manipulations of proteins of interest impact myelination.

3.1. Additional Autoradiographic Studies That Are Likely to Broaden Understanding of Peripheral Nerve Myelination

Although morphological sites of phospholipids, proteins, glycoproteins and RNA syntheses in myelinating Schwann cells have been determined, morphological sites of cholesterol, galactocerebroside and sulfatide syntheses are still unknown. Furthermore, movements of lipids and proteins from synthetic sites into myelin have only been studied for choline phospholipids [20] and fucose glycoproteins [45]. Autoradiographic studies that identify sites of cholesterol and galactolipid syntheses and that characterize and compare movements of different lipids and proteins into myelin seem warranted. Results from these studies will lay a foundation for identifying synthetic sites and characterizing movements of lipids and proteins during CNS myelination (section 3.2) for examining these processes using bio-orthogonal precursors (section 3.3) and examining how the processes are affected following injury, disease and/or gene manipulations.

Although autoradiographic studies have been carried out on cholesterol metabolism in developing, mature and regenerating rodent peripheral nerves [52–57], none have pinpointed morphological sites where myelinating Schwann cells synthesize cholesterol. To find out, if synthesis is restricted to perinuclear regions, or includes SCC/CB, we propose identifying sites of cholesterol formation at short times following tritiated acetate injection into sciatic nerves as tritiated acetate shows selectivity for cholesterol [56]. We propose examining nascent (five to twenty minutes after precursor injection) cholesterol distribution in light, electron microscope and teased fiber autoradiographs. At increased labeling times spread of cholesterol into myelin would be examined. These studies should expand on observations of Rawlins [52], who showed that within twenty minutes of intraperitoneal injection of tritiated cholesterol into sucking mice, cholesterol accumulates along outer and inner lamellae of sciatic nerve myelin sheaths. An hour later, cholesterol is spread throughout all lamellae, indicating that cholesterol moves through myelin far more rapidly than phosphatidylcholine. Proposed autoradiographic studies with intraneural injections of tritiated acetate, and tritiated cholesterol, would determine if these processes occurred in mature myelin sheaths.

Regarding galactolipids, major constituents of both central and peripheral nervous system myelin sheaths [58], tritiated sphingosine [59], tritiated galactose [60,61] and ^{35}S-sulfate [62,63] are potential precursors that could potentially provide information in autoradiographic studies on synthetic sites and movements into myelin. Conducting these experiments would depend on first showing galactolipid specificity of the precursors. Without this specificity, it might be possible to use inhibitors of protein synthesis and/or protein glycosylation to improve specificity. With specific precursors, light, electron microscope and teased fiber autoradiography could be conducted to identify synthetic sites and to follow movements into myelin.

A facet of myelin sheath dynamics worth considering is evolutionary conservation. One could find out if features of lipid and protein syntheses and movements into myelin sheaths that were characterized in rodents, were retained in birds, reptiles, amphibians, teleost and cartilaginous fishes.

 doi:10.20944/preprints202405.0549.v1

Autoradiographic studies could readily be conducted, as was done for choline lipid metabolism in frog sciatic nerves [20], using species of birds [64], reptiles [65,66], amphibians (Xenopus [67,68] and Rana [20,69]), teleost (trout [70]) and cartilaginous (little skate [71]) fishes used previously in studies of peripheral nerve myelination. Our endeavors in identifying mRNAs that co-localize with *MBP* mRNA in oligodendrocyte processes [10,12] came in part from finding that unlike in other species, in elasmobranchs, *MBP* mRNA is not enriched in oligodendrocyte processes [72].

Another possibility would be to see whether inhibiting protein synthesis and/or cholesterol synthesis would affect locations where different phospholipids, proteins, glycoproteins and possibly cholesterol and galactolipids occurred. It is known that inhibition of cholesterol synthesis in peripheral nerve blocks movements/transport of MPZ to myelin [73].

3.2. Identifying Sites of Synthesis and Movement of Myelin-Destined Lipids and Proteins during CNS Myelination

An independent study, using vesicular stomatitis virus-glycoprotein (VSV-G) to track protein movements into CNS myelin, reached a different conclusion [74] from ours. Based on their results, the investigators proposed that myelin grows by addition of proteins to inner and not outer myelin lamellae. The proposal was based on two findings: 1) Three and six hours after VSV injection into corpus callosum of twenty-day-old mice, VSV-G accumulates along inner tongue processes. 2) Myelin sheaths contain cytoplasmic channels, preserved in tissues prepared with high-pressure-freezing, freeze substitution [75]. Neither VSV-G accumulations along inner tongue processes nor are the cytoplasmic channels present in sheaths of sixty-day-old mice, suggesting that as myelination slows, this pathway shuts down. From the twenty-day mouse results, they suggested that VSV-G, a representative of myelin-destined proteins, moves through the channels to enter myelin at the inner tongue.

How might differences between our findings (protein additions to outermost lamellae) and theirs (protein additions to innermost lamellae) be reconciled? In a follow up commentary, the investigators suggested that differences may arise from differences in CNS versus PNS myelination [76], i.e., CNS myelin sheaths grow from additions to the inner lamellae whereas PNS sheaths grow from addition to the outer lamellae. Certainly, this is a testable proposal. However, other testable possibilities exist as well. Perhaps the differences reflect differences in which thinly myelinating corpus callosal sheaths grow compared with the much thicker sciatic nerve sheaths examined in our study. Another possibility is that movements of VSV-G do not reflect movements of myelin-targeted proteins. VSV-G has a large extracellular domain, and other similarly structured proteins are selectively excluded from myelin [77,78]. If VSV-G is not an appropriate probe of myelin-targeted proteins, perhaps it marks movements of proteins targeted to inner tongue processes. Not only are inner tongue processes large in myelin sheaths in the corpus callosum of twenty-day-old mice (Figures 3 and 4 [74]), but also a number of proteins, including actin [79,80], septin and anillin [81,82] and/or CAMD 4 [83–85] are selectively targeted to inner tongue processes.

Clearly further studies are needed to resolve these differences. Of two possibilities, expanding autoradiographic studies to CNS myelination or studying fate of VSV-G following injections of VSV into developing sciatic nerves, we favor the former. There are, however, several hurdles that must be addressed to get these studies working. First, compared with the research environment of fifty years ago when we began our studies and had help from colleagues conducting autoradiographic studies in neighboring labs, few, if any, labs are conducting autoradiographic studies today meaning it will be difficult to get help. Likely clearances for using radioisotopes are harder to get as well. Second, CNS tissue is morphologically far more complex than PNS tissue, making assignments of silver grains to myelin/oligodendrocyte structures far more difficult. Whereas Schwann cells myelinate single internodes well separated from one another by the extracellular space, oligodendrocytes myelinate multiple internodes that often abut one another. These morphological differences provide challenge in setting up the quantitative analyses that will be used to identify potential non perinuclear sites of lipid and protein syntheses and to characterize temporal change in grain distributions among cellular units and myelin layers readily assessed in our PNS studies (Figures 12 and 13, respectively).

 doi:10.20944/preprints202405.0549.v1

Despite these limitations, there are many reasons why we encourage investigators to conduct autoradiographic studies of CNS myelination. First, morphological sites where oligodendrocytes synthesize myelin-targeted lipids and proteins are currently unknown, and likely those sites, i.e., perinuclear regions, outer and inner tongue processes and paranodal loops are distinct enough to develop needed quantitative protocols. Second, autoradiographic studies on PNS tissues provide knowledge about a host of tritiated precursors for phospholipids, proteins, glycoproteins and RNA and if studies are expanded for cholesterol, galactolipids and sulfatides (section 3.1) that could be adapted to CNS myelination paradigms. Among phospholipid precursors, it would be of particular interest to find out if CNS axons synthesize phosphatidylinositol from injected myo-inositol precursor. Third, myelin sheaths in spinal cord are thick enough [86], to determine if proteins and lipids enter myelin at outer versus inner tongue processes. Fourth, once quantitative approaches are functioning for evaluating grain distributions during CNS myelination, they could be used in studies that look at effects of injury, disease and protein manipulations on sites of synthesis and movements from the sites into myelin.

3.3. Novel Approaches to Identify Sites Where Myelinating Cells Synthesize Proteins and Lipids, and to Characterize Their Movements to Myelin, and for Proteins to Other Internodal Locations

In part, due to the limited resolution inherent in autoradiographic approaches (sections 3.1 - 3.2), we consider an exciting alternative, non-canonical/bio-orthogonal precursors. Unfortunately, we lack practical experience with this approach and, therefore, have had to rely on multiple reviews. Fortunately, these reviews cover specifics for both proteins [87–91] and lipids [92–102]. Additionally, we point to studies that have successfully used noncanonical amino acids for proteins [103,104], and other bio-orthogonal precursors for lipids [105–107], carbohydrates [108,109] and fatty acids [98] as models to use in developing protocols for identifying synthetic sites and following movements during PNS and CNS myelination. Briefly, we focus on studies that complement autoradiographic data that have identified sites where choline, myo-inositol, amino acids and fucose are incorporated into macromolecules in myelinating Schwann cells (section 2). We believe that successes of these studies will allow expansions in ways suggested for follow up autoradiographic studies of PNS (section 3.1) and CNS (section 3.2) myelination. Finally, with a novel application, namely genetic code expansion [110], it should be possible to expand bio-orthogonal approaches to identify sites where individual proteins of interest are synthesized and to follow their movements from these sites to the internodal sites where they function.

3.3.1. Use Noncanonical/Bio-Orthogonal Precursors to Identify Sites of Phosphatidylcholine, Phosphatidylinositol, Protein and Glycoprotein Syntheses Occur in Myelinating Schwann Cells

With autoradiographic knowledge of where tritiated choline (Figures 1-3), myo-inositol (Figure 4), amino acids (Figures 6-8) and fucose (Figure 5) are incorporated into phosphatidylcholine, phosphatidylinositol, protein and glycoprotein, respectively, it seems reasonable to begin experiments using bio-orthogonal homologues to the tritiated precursors: propargylcholine for choline [105,106]), 2-*O*-(3-azidopropyl)-4,6-di-*O*-benzyl-1,3,5-methylidyne-*myo*-inositol for myo-inositol [107], azidohomoalanine and homopropargylglycine (methionine) and [89,104], β-ethynylserine (threonine) for protein [111] and a peracetylated alkynyl derivative of fucose for glycoprotein fucosylation [109]. Like autoradiographic studies, these precursors would be injected into exposed sciatic nerves of two-to-three-month-old mice. At twenty minutes and two hours, nerves would be fixed *in situ,* excised, washed to remove unincorporated precursors and soluble metabolites, embedded and prepared for transverse, longitudinal and teased fiber examination. Macromolecular products would then be visualized with fluorescent molecules added using 'click' chemistry, e.g., [112,113], and with procedures used for viewing by electron microscopy, e.g., [114,115]. Not only should these studies confirm the distribution patterns seen for nascent phosphatidylcholine, phosphatidylinositol, protein and glycoprotein, but at higher resolutions.

 doi:10.20944/preprints202405.0549.v1

3.3.2. Using the Bio-Orthogonal Precursor Approach to Follow Movements of Phospholipids, Proteins and Glycoproteins into PNS and CNS Myelin Sheaths

Success in studies that identify sites where bio-orthogonal precursors are incorporated into phosphatidylcholine, phosphatidylinositol, proteins and glycoproteins (section 3.3.1), should be followed with studies comparable to those described for follow up autoradiographic studies (sections 3.1 – 3.2). Suggested studies with bio-orthogonal precursors would include: 1) Examination of sciatic nerves fixed after longer survival to characterize movements of phosphatidylcholine, phosphatidylinositol, proteins and glycoproteins from synthetic sites into myelin sheaths. Hopefully, improved resolution (from ~twenty lamellae (autoradiography) to single lamellae (bio-orthogonal precursors), high-resolution data could be generated on movements of macromolecules into fibers, sorted by myelin sheath thickness and/or fiber caliber to find out if differences occurred in entry and movements based on these parameters. 2) Use the same precursors to identify where phosphatidylcholine, phosphatidylinositol, protein and glycoprotein are synthesized in myelinating oligodendrocytes. With improved resolution, studies would not be limited to tissues containing thick myelin sheaths, e.g., spinal cord white matter, but include structurally well-organized optic nerve and corpus callosum, the latter to use in comparison with VSV-G results. 3) Use other bio-orthogonal precursors to identify sites where other phospholipids, cholesterol, galactocerebroside and sulfatide are synthesized in CNS and PNS and characterize movements from these sites into and through myelin. 4) Use these precursors *in vitro* settings, e.g., neuron-Schwann cell co-cultures [116–120], oligodendrocyte-neuron co-cultures [121–125], brain and spinal cord slice preparations and brain and spinal cord organoids [126–128]. Improved resolution will enable these expansions. 5) Expand the studies to injury and disease models and to situations in which genes/proteins of interest are modified.

3.3.3. Using Genetic Code Expansion to Identify Sites Where Proteins of Interest Are Synthesized and to Follow Movements from These Sites to Sites of Residence

In addition to using bio-orthogonal precursors for amino acids that incorporate into all proteins, current approaches have gone a step further in using genetic code expansion to target bio-orthogonal amino acids to specific sites of proteins of interest [110,129–133]. Because this approach is mostly carried out under *in vitro* conditions, it would seem reasonable to study trafficking of proteins of interest in the *in vitro* conditions examine in the previous (3.4.2). With development of a genetic code expansion approach, it should be possible to locate sites where proteins located at paranodes, e.g. claudin-11 in CNS [134,135] and claudin-19 in PNS [136], E-cadherin in PNS [137], gliomedin in PNS microvilli [138], and along adaxonal sites, e.g., CADM4 [83,84], septin and anillin filaments [81,82], to name a few. There is precedence in a study that examined expressions of neurofascin-186 and sodium channel (Nav1.6) to axon initial segments in cultured hippocampal neurons [139]. Although a lot of work will be required to get these approaches up and running, it is likely they will pay big dividends in obtaining novel insights in ways myelinating cells for and maintain their internodes.

4. Conclusions

A major goal of this review is to provide awareness of approaches that: 1) identify sites where myelinating cells, oligodendrocytes and Schwann cells, synthesize proteins and lipids targeted to compact myelin and 2) follow and characterize movements of these constituents from synthetic sites into myelin. Studies of this nature, at least at the morphological level have been limited to autoradiographic studies carried out decades ago. Reviewing these studies and considering further autoradiographic and non-autoradiographic approaches, we hope will encourage investigators to conduct studies that will uncover understudied spatial and temporal aspects of myelination.

Author Contributions: RMG wrote the review and prepared the figures. AG helped revise the manuscript and the figures.

Funding: This research received no external funding.

 doi:10.20944/preprints202405.0549.v1

Data Availability Statement: Figures 1 – 11 are modified from original publications and are shown with permissions from the publishers of the original articles. Figures 12 and 13 are prepared for this publication with data from tables in original publications as cited.

Conflicts of Interest: The authors declare no conflicts of interest.

References

1. Benjamins, J.A.; Gray, M.; Morell, P. Metabolic relations between myelin subfractions: entry of proteins. *Journal of Neurochemistry* **1976**, *27*, 571-575.
2. Colman, D.R.; Kreibich, G.; Frey, A.B.; Sabatini, D.D. Synthesis and incorporation of myelin polypeptides into CNS myelin. *Journal of Cell Biology* **1982**, *95*, 598-608.
3. Nussbaum, J.L.; Roussel, G. Immunocytochemical demonstration of the transport of myelin proteolipids through the Golgi apparatus. *Cell Tissue Res* **1983**, *234*, 547-559.
4. Trapp, B.D.; Moench, M.; Pulley, E.; Barbosa, E.; Tennekoon, G.I.; Griffin, J. Spatial segregation of mRNA encoding myelin-specific proteins. *Proceedings of the National Academy of Sciences USAI.Acad.Sci.USA* **1987**, *84*, 7773-7777.
5. Rapaport, R.N.; Benjamins, J.A. Kinetics of entry of P 0 protein into peripheral nerve myelin. *Journal of Neurochemistry* **1981**, *37*, 161-171.
6. Trapp, B.D.; Hauer, P.; Lemke, G. Axonal regulation of myelin protein mRNA levels in actively myelinating Schwann cells. *Journal of Neuroscience* **1988**, *8*, 3515-3521.
7. Griffiths, I.R.; Mitchell, L.S.; McPhilemy, K.; Morrison, S.; Kyriakides, E.; Barrie, J.A. Expression of myelin protein genes in Schwann cells. *Journal of Neurocytology* **1989**, *18*, 345-352.
8. Gould, R.M.; Holshek, J.; Silverman, W.; Spivack, W. Localization of phospholipid synthesis to Schwann cells and axons. *Journal of Neurochemistry* **1987**, *48*, 1121-1131.
9. Gould, R.M.; Mattingly, G. Regional localization of RNA, protein and lipid metabolism in Schwann cells in vivo. *Journal of Neurocytology* **1990**, *19*, 285-301.
10. Gould, R.M.; Freund, C.M.; Palmer, F.; Feinstein, D.L. Messenger RNAs located at sites of myelin assembly. *Journal of Neurochemistry* **2000**, *75*, 1834-1844.
11. Holz, A.; Schaeren-Wiemers, N.; Schaefer, C.; Pott, U.; Colello, R.J.; Schwab, M.E. Molecular and developmental characterization of novel cDNAs of the myelin-associated oligodendrocytic basic protein. *Journal of Neuroscience* **1996**, *16*, 467-477.
12. Gould, R.; Brady, S. Identifying mRNAs Residing in Myelinating Oligodendrocyte Processes as a Basis for Understanding Internode Autonomy. *Life (Basel)* **2023**, *13*, doi:10.3390/life13040945.
13. Waehneldt, T.V. Phylogeny of myelin proteins. *Ann.NY Acad.Sci.* **1990**, *605*, 15-28.
14. Gould, R.M.; Oakley, T.; Goldstone, J.V.; Dugas, J.C.; Brady, S.T.; Gow, A. Myelin sheaths are formed with proteins that originated in vertebrate lineages. *Neuron Glia Biol* **2008**, *4*, 137-152, doi:10.1017/S1740925X09990238.
15. O'Brien, J.S.; Sampson, E.L.; Stern, M.B. Lipid composition of myelin from the peripheral nervous system. Intradural spinal roots. *J Neurochem* **1967**, *14*, 357-365, doi:10.1111/j.1471-4159.1967.tb09532.x.
16. MacBrinn, M.C.; O'Brien, J.S. Lipid composition of optic nerve myelin. *J Neurochem* **1969**, *16*, 7-12, doi:10.1111/j.1471-4159.1969.tb10337.x.
17. O'Brien, J.S.; Sampson, E.L. Lipid composition of the normal human brain: gray matter, white matter, and myelin. *Journal of Lipid Research* **1965**, *6*, 537-544.
18. Wang, C.; Palavicini, J.P.; Han, X. Lipidomics Profiling of Myelin. *Methods Mol Biol* **2018**, *1791*, 37-50, doi:10.1007/978-1-4939-7862-5_4.
19. Cermenati, G.; Mitro, N.; Audano, M.; Melcangi, R.C.; Crestani, M.; De Fabiani, E.; Caruso, D. Lipids in the nervous system: from biochemistry and molecular biology to patho-physiology. *Biochim Biophys Acta* **2015**, *1851*, 51-60, doi:10.1016/j.bbalip.2014.08.011.
20. Gould, R.M.; Dawson, R.M.C. Incorporation of newly formed lecithin into peripheral nerve myelin. *Journal of Cell Biology* **1976**, *68*, 480-496.
21. Gould, R.M.; Sinatra, R.S. Internodal distribution of phosphatidylcholine biosynthetic activity in teased peripheral nerve fibers: An autoradiographic study. *Journal of Neurocytology* **1981**, *10*, 161-167.
22. Gould, R.M. Inositol lipid synthesis localized in axons and unmyelinated fibers of peripheral nerve. *Brain Research* **1976**, *117*, 169.

23. Kremser, C.; Klemm, A.L.; van Uelft, M.; Imgrund, S.; Ginkel, C.; Hartmann, D.; Willecke, K. Cell-type-specific expression pattern of ceramide synthase 2 protein in mouse tissues. *Histochem Cell Biol* **2013**, *140*, 533-547, doi:10.1007/s00418-013-1091-z.
24. Peters, A.; Palay, S.L.; Webster, H.d. *The fine structure of the nervous system: Neurons and their supporting cells*; Oxford University Press: New York, 1991; pp. 3-494.
25. McKenna, O.; Arnold, G.; Holtzman, E. Microperoxisome distribution in the central nervous system of the rat. *Brain Res* **1976**, *117*, 181-194, doi:10.1016/0006-8993(76)90729-0.
26. Kassmann, C.M. Myelin peroxisomes - essential organelles for the maintenance of white matter in the nervous system. *Biochimie* **2014**, *98*, 111-118, doi:10.1016/j.biochi.2013.09.020.
27. Meyer, N.; Rinholm, J.E. Mitochondria in Myelinating Oligodendrocytes: Slow and Out of Breath? *Metabolites* **2021**, *11*, doi:10.3390/metabo11060359.
28. Rinholm, J.E.; Vervaeke, K.; Tadross, M.R.; Tkachuk, A.N.; Kopek, B.G.; Brown, T.A.; Bergersen, L.H.; Clayton, D.A. Movement and structure of mitochondria in oligodendrocytes and their myelin sheaths. *Glia* **2016**, *64*, 810-825, doi:10.1002/glia.22965.
29. Nakamura, D.S.; Lin, Y.H.; Khan, D.; Gothie, J.M.; de Faria, O., Jr.; Dixon, J.A.; McBride, H.M.; Antel, J.P.; Kennedy, T.E. Mitochondrial dynamics and bioenergetics regulated by netrin-1 in oligodendrocytes. *Glia* **2021**, *69*, 392-412, doi:10.1002/glia.23905.
30. Schmitt, S.; Cantuti Castelvetri, L.; Simons, M. Metabolism and functions of lipids in myelin. *Biochim Biophys Acta* **2015**, *1851*, 999-1005, doi:10.1016/j.bbalip.2014.12.016.
31. Miller, E.K.; Dawson, R.M.C. Can mitochondria and synaptosomes of guinea-pig brain synthesize phospholipids? *Biochemical Journal* **1972**, *126*, 805-821.
32. Davison, A.N.; Peters, A. The biochemistry of the myelin sheath. In *Myelination*, Charles C. Thomas: Springfield,IL, 1970; pp. 80-161.
33. Hendelman, W.J.; Bunge, R.P. Radioautographic studies of choline incorporation into peripheral nerve myelin. *J Cell Biol* **1969**, *40*, 190-208, doi:10.1083/jcb.40.1.190.
34. Stein, O.; Stein, Y. LIPID SYNTHESIS, INTRACELLULAR TRANSPORT, AND STORAGE : III. Electron Microscopic Radioautographic Study of the Rat Heart Perfused with Tritiated Oleic Acid. *J Cell Biol* **1968**, *36*, 63-77.
35. Stein, O.; Stein, Y. Lipid synthesis, intracellular transport, and secretion. II. Electron microscopic radioautographic study of the mouse lactating mammary gland. *J Cell Biol* **1967**, *34*, 251-263, doi:10.1083/jcb.34.1.251.
36. Stein, O.; Stein, Y. Lipid synthesis, intracellular transport, storage, and secretion. I. Electron microscopic radioautographic study of liver after injection of tritiated palmitate or glycerol in fasted and ethanol-treated rats. *J Cell Biol* **1967**, *33*, 319-339, doi:10.1083/jcb.33.2.319.
37. Court, F.A.; Sherman, D.L.; Pratt, T.; Garry, E.M.; Ribchester, R.R.; Cottrell, D.F.; Fleetwood-Walker, S.M.; Brophy, P.J. Restricted growth of Schwann cells lacking Cajal bands slows conduction in myelinated nerves. *Nature* **2004**, *431*, 191-195.
38. Gould, R.M.; Connell, F.; Spivack, W. Phospholipid metabolism in mouse sciatic nerve in vivo. *Journal of Neurochemistry* **1987**, *48*, 853-859.
39. Sima, A.A.; Dunlap, J.A.; Davidson, E.P.; Wiese, T.J.; Lightle, R.L.; Greene, D.A.; Yorek, M.A. Supplemental myo-inositol prevents L-fucose-induced diabetic neuropathy. *Diabetes* **1997**, *46*, 301-306, doi:10.2337/diab.46.2.301.
40. Kumara-Siri, M.H.; Gould, R.M. Enzymes of phospholipid synthesis: axonal vs. Schwann cell distribution. *Brain Research* **1980**, *186*, 315-330.
41. Larrabee, M.G.; Brinley, F.J. Incorporation of labelled phosphate into phospholipids in squid giant axons. *Journal of Neurochemistry* **1968**, *15*, 533-545.
42. Gould, R.M.; Pant, H.; Gainer, H.; Tytell, M. Phospholipid synthesis in the squid giant axon: incorporation of lipid precursors. *Journal of Neurochemistry* **1983**, *40*, 1293-1299.
43. Gould, R.M.; Spivack, W.; Robertson, D.; Poznansky, M.J. Phospholipid synthesis in the squid giant axon: enzymes of phosphatidylinositol metabolism. *Journal of Neurochemistry* **1983**, *40*, 1300-1306.
44. Everly, J.L.; Brady, R.O.; Quarles, R.H. Evidence that the major protein in rat sciatic nerve myelin is a glycoprotein. *Journal of Neurochemistry* **1973**, *21*, 329-334.
45. Gould, R.M. Incorporation of glycoproteins into peripheral nerve myelin. *Journal of Cell Biology* **1977**, *75*, 326-339.

46. Gould, R.M. Metabolic organization of the myelinating Schwann cell. *Annals of the New York Academy of Sciences* **1990**, *605*, 44-54.
47. Toews, A.D.; Saunders, B.F.; Morell, P. Axonal transport and metabolism of glycoproteins in rat sciatic nerve. *J Neurochem* **1982**, *39*, 1348-1355, doi:10.1111/j.1471-4159.1982.tb12577.x.
48. Ainger, K.; Avossa, D.; Morgan, F.; Hill, S.J.; Barry, C.; Barbarese, E.; Carson, J.H. Transport and localization of exogenous myelin basic protein mRNA microinjected into oligodendrocytes. *Journal of Cell Biology* **1993**, *123*, 431-441.
49. Davis, L.G.; Banker, G.A.; Steward, O. Selective dendritic transport of RNA in Hippocampal neurons in culture. *Nature* **1987**, *330*, 477-479.
50. Williams, M. The assessment of electron microscope autoradiographs. *Adv Opt Electron Microsc* **1969**, *3*, 219-272.
51. Williams, M. Electron microscopic autoradiography: its application to protein biosynthesis. *Techniques in protein biosynthesis* **1973**, *3*, 126-190.
52. Rawlins, F.A. A time-sequence autoradiographic study of the in vivo incorporation of [1,2- 3 H-cholesterol into peripheral nerve myelin. *Journal of Cell Biology* **1973**, *58*, 42-53.
53. Goodrum, J.F.; Brown, J.C.; Fowler, K.A.; Bouldin, T.W. Axonal regeneration, but not myelination, is partially dependent on local cholesterol reutilization in regenerating nerve. *J Neuropathol Exp Neurol* **2000**, *59*, 1002-1010, doi:10.1093/jnen/59.11.1002.
54. Goodrum, J.F. Cholesterol from degenerating nerve myelin becomes associated with lipoproteins containing apolipoprotein E. *Journal of Neurochemistry* **1991**, *56*, 2082-2086.
55. Goodrum, J.F.; Pentchev, P.G. Cholesterol reutilization during myelination of regenerating PNS axons is impaired in Niemann-Pick disease type C mice. *J Neurosci Res* **1997**, *49*, 389-392, doi:10.1002/(sici)1097-4547(19970801)49:3<389::aid-jnr14>3.0.co;2-v.
56. Goodrum, J.F. Cholesterol synthesis is down-regulated during regeneration of peripheral nerve. *J Neurochem* **1990**, *54*, 1709-1715, doi:10.1111/j.1471-4159.1990.tb01225.x.
57. Fu, Q.; Goodrum, J.F.; Hayes, C.; Hostettler, J.D.; Toews, A.D.; Morell, P. Control of cholesterol biosynthesis in Schwann cells. *Journal of Neurochemistry* **1998**, *71*, 549-555.
58. Chrast, R.; Saher, G.; Nave, K.A.; Verheijen, M.H. Lipid metabolism in myelinating glial cells: lessons from human inherited disorders and mouse models. *Journal of Lipid Research* **2011**, *52*, 419-434, doi:10.1194/jlr.R009761.
59. Dolo, V.; D'Ascenzo, S.; Sorice, M.; Pavan, A.; Sciannamblo, M.; Prinetti, A.; Chigorno, V.; Tettamanti, G.; Sonnino, S. New approaches to the study of sphingolipid enriched membrane domains: the use of electron microscopic autoradiography to reveal metabolically tritium labeled sphingolipids in cell cultures. *Glycoconj J* **2000**, *17*, 261-268, doi:10.1023/a:1026505710607.
60. Pleasure, D.; Parris, J.; Stern, J.; Grinspan, J.; Kim, S.U. Incorporation of tritiated galactose into galactocerebroside by cultured rat oligodendrocytes: effects of cyclic adenosine 3',5'-monophosphate analogues. *J Neurochem* **1986**, *46*, 300-302, doi:10.1111/j.1471-4159.1986.tb12963.x.
61. Whur, P.; Herscovics, A.; Leblond, C.P. Radioautographic visualization of the incorporation of galactose-3H and mannose-3H by rat thyroids in vitro in relation to the stages of thyroglobulin synthesis. *J Cell Biol* **1969**, *43*, 289-311, doi:10.1083/jcb.43.2.289.
62. Young, R.W. The role of the Golgi complex in sulfate metabolism. *Journal of Cell Biology* **1973**, *57*, 175-189.
63. Tennekoon, G.I.; Cohen, S.R.; Price, D.L.; McKhann, G.M. Myelinogenesis in optic nerve. A morphological, autoradiographic, and biochemical analysis. *J Cell Biol* **1977**, *72*, 604-616, doi:10.1083/jcb.72.3.604.
64. Oulton, M.R.; Mezei, C. Characterization of myelin of chick sciatic nerve during development. *J Lipid Res* **1976**, *17*, 167-175.
65. Robertson, J.D. The ultrastructure of adult vertebrate peripheral myelinated nerve in relation to myelinogenesis. *Journal of Biophysical and Biochemical Cytology* **1955**, *1*, 271.
66. Nadon, N.L.; Crotzer, D.R.; Stewart, J.R. Embryonic development of central nervous system myelination in a reptilian species, Eumeces fasciatus. *Journal of Comparative Neurology* **1995**, *362*, 433-440.
67. Kaya, F.; Mannioui, A.; Chesneau, A.; Sekizar, S.; Maillard, E.; Ballagny, C.; Houel-Renault, L.; Dupasquier, D.; Bronchain, O.; Holtzmann, I., et al. Live imaging of targeted cell ablation in Xenopus: a new model to study demyelination and repair. *J Neurosci* **2012**, *32*, 12885-12895, doi:10.1523/JNEUROSCI.2252-12.2012.

68. Luo, X.; Cerullo, J.; Dawli, T.; Priest, C.; Haddadin, Z.; Kim, A.; Inouye, H.; Suffoletto, B.P.; Avila, R.L.; Lees, J.P., et al. Peripheral myelin of Xenopus laevis: Role of electrostatic and hydrophobic interactions in membrane compaction. *J Struct.Biol.* **2007**.
69. Uhrik, B.; Stampfli, R. Ultrastructural observations on nodes of Ranvier from isolated single frog peripheral nerve fibres. *Brain Res.* **1981**, *215*, 93-101.
70. Jeserich, G.; Waehneldt, T.V. Bony fish myelin: evidence for common major structural glycoproteins in central and peripheral myelin of trout. *Journal of Neurochemistry* **1986**, *46*, 525-533.
71. Möbius, W.; Hümmert, S.; Ruhwedel, T.; Kuzirian, A.; Gould, R. New Species Can Broaden Myelin Research: Suitability of Little Skate, Leucoraja erinacea. *Life* **2021**, *11*, 136.
72. Pahl, N.; Homsi, S.; Morrison, H.G.; Gould, R.M. mRNAs located in Squalus acanthias (spiny dogfish) oligodendrocyte processes. *Biological Bulletin* **2002**, *203*, 217-218.
73. Saher, G.; Quintes, S.; Mobius, W.; Wehr, M.C.; Kramer-Albers, E.M.; Brugger, B.; Nave, K.A. Cholesterol regulates the endoplasmic reticulum exit of the major membrane protein P0 required for peripheral myelin compaction. *J Neurosci* **2009**, *29*, 6094-6104, doi:29/19/6094 [pii]10.1523/JNEUROSCI.0686-09.2009.
74. Snaidero, N.; Mobius, W.; Czopka, T.; Hekking, L.H.; Mathisen, C.; Verkleij, D.; Goebbels, S.; Edgar, J.; Merkler, D.; Lyons, D.A., et al. Myelin Membrane Wrapping of CNS Axons by PI(3,4,5)P3-Dependent Polarized Growth at the Inner Tongue. *Cell* **2014**, *156*, 277-290, doi:10.1016/j.cell.2013.11.044.
75. Mobius, W.; Nave, K.A.; Werner, H.B. Electron microscopy of myelin: Structure preservation by high-pressure freezing. *Brain Res* **2016**, *1641*, 92-100, doi:10.1016/j.brainres.2016.02.027.
76. Snaidero, N.; Simons, M. Myelination at a glance. *J Cell Sci* **2014**, *127*, 2999-3004, doi:10.1242/jcs.151043.
77. Bakhti, M.; Aggarwal, S.; Simons, M. Myelin architecture: zippering membranes tightly together. *Cell Mol Life Sci* **2014**, *71*, 1265-1277, doi:10.1007/s00018-013-1492-0.
78. Aggarwal, S.; Yurlova, L.; Snaidero, N.; Reetz, C.; Frey, S.; Zimmermann, J.; Pahler, G.; Janshoff, A.; Friedrichs, J.; Muller, D.J., et al. A size barrier limits protein diffusion at the cell surface to generate lipid-rich myelin-membrane sheets. *Dev Cell* **2011**, *21*, 445-456, doi:S1534-5807(11)00313-3 [pii]10.1016/j.devcel.2011.08.001.
79. Zuchero, J.B.; Fu, M.-m.; Sloan, Steven A.; Ibrahim, A.; Olson, A.; Zaremba, A.; Dugas, Jason C.; Wienbar, S.; Caprariello, Andrew V.; Kantor, C., et al. CNS Myelin Wrapping Is Driven by Actin Disassembly. *Developmental Cell* **2015**, *34*, 152-167, doi:http://dx.doi.org/10.1016/j.devcel.2015.06.011.
80. Nawaz, S.; Sánchez, P.; Schmitt, S.; Snaidero, N.; Mitkovski, M.; Velte, C.; Brückner, Bastian R.; Alexopoulos, I.; Czopka, T.; Jung, Sang Y., et al. Actin Filament Turnover Drives Leading Edge Growth during Myelin Sheath Formation in the Central Nervous System. *Developmental Cell* **2015**, *34*, 139-151, doi:http://dx.doi.org/10.1016/j.devcel.2015.05.013.
81. Erwig, M.S.; Patzig, J.; Steyer, A.M.; Dibaj, P.; Heilmann, M.; Heilmann, I.; Jung, R.B.; Kusch, K.; Mobius, W.; Jahn, O., et al. Anillin facilitates septin assembly to prevent pathological outfoldings of central nervous system myelin. *eLife* **2019**, *8*, doi:10.7554/eLife.43888.
82. Patzig, J.; Erwig, M.S.; Tenzer, S.; Kusch, K.; Dibaj, P.; Möbius, W.; Goebbels, S.; Schaeren-Wiemers, N.; Nave, K.-A.; Werner, H.B. Septin/anillin filaments scaffold central nervous system myelin to accelerate nerve conduction. *eLife* **2016**, *5*, e17119, doi:10.7554/eLife.17119.
83. Maurel, P.; Einheber, S.; Galinska, J.; Thaker, P.; Lam, I.; Rubin, M.B.; Scherer, S.S.; Murakami, Y.; Gutmann, D.H.; Salzer, J.L. Nectin-like proteins mediate axon Schwann cell interactions along the internode and are essential for myelination. *J Cell Biol.* **2007**, *178*, 861-874.
84. Spiegel, I.; Adamsky, K.; Eshed, Y.; Milo, R.; Sabanay, H.; Sarig-Nadir, O.; Horresh, I.; Scherer, S.S.; Rasband, M.N.; Peles, E. A central role for Necl4 (SynCAM4) in Schwann cell-axon interaction and myelination. *Nat Neurosci* **2007**, *10*, 861-869.
85. Pellissier, F.; Gerber, A.; Bauer, C.; Ballivet, M.; Ossipow, V. The adhesion molecule Necl-3/SynCAM-2 localizes to myelinated axons, binds to oligodendrocytes and promotes cell adhesion. *BMC Neurosci* **2007**, *8*, 90, doi:10.1186/1471-2202-8-90.
86. Schwab, M.E.; Schnell, L. Region-specific appearance of myelin constituents in the developing rat spinal cord. *Journal of Neurocytology* **1989**, *18*, 161-169.
87. Elia, N. Using unnatural amino acids to selectively label proteins for cellular imaging: a cell biologist viewpoint. *Febs J* **2021**, *288*, 1107-1117, doi:10.1111/febs.15477.
88. Hinz, F.I.; Dieterich, D.C.; Schuman, E.M. Teaching old NCATs new tricks: using non-canonical amino acid tagging to study neuronal plasticity. *Curr Opin Chem Biol* **2013**, *17*, 738-746, doi:10.1016/j.cbpa.2013.07.021.

89. Lang, K.; Chin, J.W. Cellular incorporation of unnatural amino acids and bioorthogonal labeling of proteins. *Chemical reviews* **2014**, *114*, 4764-4806, doi:10.1021/cr400355w.
90. Lee, K.J.; Kang, D.; Park, H.S. Site-Specific Labeling of Proteins Using Unnatural Amino Acids. *Molecules and cells* **2019**, *42*, 386-396, doi:10.14348/molcells.2019.0078.
91. Leisle, L.; Valiyaveetil, F.; Mehl, R.A.; Ahern, C.A. Incorporation of Non-Canonical Amino Acids. *Adv Exp Med Biol* **2015**, *869*, 119-151, doi:10.1007/978-1-4939-2845-3_7.
92. Dadina, N.; Tyson, J.; Zheng, S.; Lesiak, L.; Schepartz, A. Imaging organelle membranes in live cells at the nanoscale with lipid-based fluorescent probes. *Curr Opin Chem Biol* **2021**, *65*, 154-162, doi:10.1016/j.cbpa.2021.09.003.
93. Daemen, S.; van Zandvoort, M.; Parekh, S.H.; Hesselink, M.K.C. Microscopy tools for the investigation of intracellular lipid storage and dynamics. *Mol Metab* **2016**, *5*, 153-163, doi:10.1016/j.molmet.2015.12.005.
94. Flores, J.; White, B.M.; Brea, R.J.; Baskin, J.M.; Devaraj, N.K. Lipids: chemical tools for their synthesis, modification, and analysis. *Chem Soc Rev* **2020**, *49*, 4602-4614, doi:10.1039/d0cs00154f.
95. Klymchenko, A.S. Fluorescent Probes for Lipid Membranes: From the Cell Surface to Organelles. *Acc Chem Res* **2023**, *56*, 1-12, doi:10.1021/acs.accounts.2c00586.
96. Hang, H.C.; Wilson, J.P.; Charron, G. Bioorthogonal chemical reporters for analyzing protein lipidation and lipid trafficking. *Acc Chem Res* **2011**, *44*, 699-708, doi:10.1021/ar200063v.
97. Knittel, C.H.; Devaraj, N.K. Bioconjugation Strategies for Revealing the Roles of Lipids in Living Cells. *Acc Chem Res* **2022**, *55*, 3099-3109, doi:10.1021/acs.accounts.2c00511.
98. Kuerschner, L.; Leyendecker, P.; Klizaite, K.; Fiedler, M.; Saam, J.; Thiele, C. Development of oxaalkyne and alkyne fatty acids as novel tracers to study fatty acid beta-oxidation pathways and intermediates. *J Lipid Res* **2022**, *63*, 100188, doi:10.1016/j.jlr.2022.100188.
99. Punt, J.M.; van der Vliet, D.; van der Stelt, M. Chemical Probes to Control and Visualize Lipid Metabolism in the Brain. *Acc Chem Res* **2022**, *55*, 3205-3217, doi:10.1021/acs.accounts.2c00521.
100. Shanbhag, K.; Sharma, K.; Kamat, S.S. Photoreactive bioorthogonal lipid probes and their applications in mammalian biology. *RSC Chem Biol* **2023**, *4*, 37-46, doi:10.1039/d2cb00174h.
101. Tamura, T.; Hamachi, I. Chemical biology tools for imaging-based analysis of organelle membranes and lipids. *Current Opinion in Chemical Biology* **2022**, *70*, 102182.
102. Zheng, S.; Dadina, N.; Mozumdar, D.; Lesiak, L.; Martinez, K.N.; Miller, E.W.; Schepartz, A. Long-term super-resolution inner mitochondrial membrane imaging with a lipid probe. *Nat Chem Biol* **2023**, 10.1038/s41589-023-01450-y, doi:10.1038/s41589-023-01450-y.
103. Ngo, J.T.; Tirrell, D.A. Noncanonical amino acids in the interrogation of cellular protein synthesis. *Acc Chem Res* **2011**, *44*, 677-685, doi:10.1021/ar200144y.
104. Dieterich, D.C.; Hodas, J.J.; Gouzer, G.; Shadrin, I.Y.; Ngo, J.T.; Triller, A.; Tirrell, D.A.; Schuman, E.M. In situ visualization and dynamics of newly synthesized proteins in rat hippocampal neurons. *Nat Neurosci* **2010**, *13*, 897-905, doi:10.1038/nn.2580.
105. Ancajas, C.F.; Ricks, T.J.; Best, M.D. Metabolic labeling of glycerophospholipids via clickable analogs derivatized at the lipid headgroup. *Chem Phys Lipids* **2020**, *232*, 104971, doi:10.1016/j.chemphyslip.2020.104971.
106. Jao, C.Y.; Roth, M.; Welti, R.; Salic, A. Metabolic labeling and direct imaging of choline phospholipids in vivo. *Proc Natl Acad Sci U S A* **2009**, *106*, 15332-15337, doi:10.1073/pnas.0907864106.
107. Ricks, T.J.; Cassilly, C.D.; Carr, A.J.; Alves, D.S.; Alam, S.; Tscherch, K.; Yokley, T.W.; Workman, C.E.; Morrell-Falvey, J.L.; Barrera, F.N., et al. Labeling of Phosphatidylinositol Lipid Products in Cells through Metabolic Engineering by Using a Clickable myo-Inositol Probe. *Chembiochem* **2019**, *20*, 172-180, doi:10.1002/cbic.201800248.
108. Bird, R.E.; Lemmel, S.A.; Yu, X.; Zhou, Q.A. Bioorthogonal Chemistry and Its Applications. *Bioconjug Chem* **2021**, *32*, 2457-2479, doi:10.1021/acs.bioconjchem.1c00461.
109. Hsu, T.L.; Hanson, S.R.; Kishikawa, K.; Wang, S.K.; Sawa, M.; Wong, C.H. Alkynyl sugar analogs for the labeling and visualization of glycoconjugates in cells. *Proc Natl Acad Sci U S A* **2007**, *104*, 2614-2619, doi:10.1073/pnas.0611307104.
110. Chung, C.Z.; Amikura, K.; Soll, D. Using Genetic Code Expansion for Protein Biochemical Studies. *Front Bioeng Biotechnol* **2020**, *8*, 598577, doi:10.3389/fbioe.2020.598577.

111. Ignacio, B.J.; Dijkstra, J.; Mora, N.; Slot, E.F.J.; van Weijsten, M.J.; Storkebaum, E.; Vermeulen, M.; Bonger, K.M. THRONCAT: metabolic labeling of newly synthesized proteins using a bioorthogonal threonine analog. *Nat Commun* **2023**, *14*, 3367, doi:10.1038/s41467-023-39063-7.
112. Carlisle, A.K.; Gotz, J.; Bodea, L.G. Three methods for examining the de novo proteome of microglia using BONCAT bioorthogonal labeling and FUNCAT click chemistry. *STAR Protoc* **2023**, *4*, 102418, doi:10.1016/j.xpro.2023.102418.
113. Kharod, S.C.; Monday, H.R.; Yoon, Y.J.; Castillo, P.E. Protocol to study presynaptic protein synthesis in ex vivo mouse hippocampal slices using HaloTag technology. *STAR Protoc* **2023**, *4*, 101986, doi:10.1016/j.xpro.2022.101986.
114. Ngo, J.T.; Adams, S.R.; Deerinck, T.J.; Boassa, D.; Rodriguez-Rivera, F.; Palida, S.F.; Bertozzi, C.R.; Ellisman, M.H.; Tsien, R.Y. Click-EM for imaging metabolically tagged nonprotein biomolecules. *Nat Chem Biol* **2016**, *12*, 459-465, doi:10.1038/nchembio.2076.
115. Pope, I.; Tanner, H.; Masia, F.; Payne, L.; Arkill, K.P.; Mantell, J.; Langbein, W.; Borri, P.; Verkade, P. Correlative light-electron microscopy using small gold nanoparticles as single probes. *Light Sci Appl* **2023**, *12*, 80, doi:10.1038/s41377-023-01115-4.
116. Bunge, R.P.; Bunge, M.B.; Bates, M. Movements of the Schwann cell nucleus implicate progression of the inner (axon-related) Schwann cell process during myelination. *Journal of Cell Biology* **1989**, *109*, 273-284.
117. Sango, K.; Kawakami, E.; Yanagisawa, H.; Takaku, S.; Tsukamoto, M.; Utsunomiya, K.; Watabe, K. Myelination in coculture of established neuronal and Schwann cell lines. *Histochemistry and cell biology* **2012**, *137*, 829-839.
118. Mutschler, C.; Fazal, S.V.; Schumacher, N.; Loreto, A.; Coleman, M.P.; Arthur-Farraj, P. Schwann cells are axo-protective after injury irrespective of myelination status in mouse Schwann cell-neuron cocultures. *J Cell Sci* **2023**, *136*, doi:10.1242/jcs.261557.
119. Booth, D.G.; Beckett, A.J.; Prior, I.A.; Meijer, D. SuperCLEM: an accessible correlative light and electron microscopy approach for investigation of neurons and glia in vitro. *Biology open* **2019**, *8*, doi:10.1242/bio.042085.
120. Podratz, J.L.; Rodriguez, E.; Windebank, A.J. Role of the extracellular matrix in myelination of peripheral nerve. *Glia* **2001**, *35*, 35-40.
121. Ristola, M.; Sukki, L.; Azevedo, M.M.; Seixas, A.I.; Relvas, J.B.; Narkilahti, S.; Kallio, P. A compartmentalized neuron-oligodendrocyte co-culture device for myelin research: design, fabrication and functionality testing. *Journal of Micromechanics and Microengineering* **2019**, *29*, 065009.
122. Jarjour, A.A.; Zhang, H.; Bauer, N.; Ffrench-Constant, C.; Williams, A. In vitro modeling of central nervous system myelination and remyelination. *Glia* **2012**, *60*, 1-12, doi:10.1002/glia.21231.
123. Pang, Y.; Zheng, B.; Kimberly, S.L.; Cai, Z.; Rhodes, P.G.; Lin, R.C. Neuron-oligodendrocyte myelination co-culture derived from embryonic rat spinal cord and cerebral cortex. *Brain Behav* **2012**, *2*, 53-67, doi:10.1002/brb3.33.
124. Wang, Z.; Colognato, H.; ffrench-Constant, C. Contrasting effects of mitogenic growth factors on myelination in neuron-oligodendrocyte co-cultures. *Glia* **2007**, *55*, 537-545.
125. Gardner, A.; Jukkola, P.; Gu, C. Myelination of rodent hippocampal neurons in culture. *Nat Protoc* **2012**, *7*, 1774-1782, doi:10.1038/nprot.2012.100.
126. James, O.G.; Selvaraj, B.T.; Magnani, D.; Burr, K.; Connick, P.; Barton, S.K.; Vasistha, N.A.; Hampton, D.W.; Story, D.; Smigiel, R., et al. iPSC-derived myelinoids to study myelin biology of humans. *Dev Cell* **2021**, *56*, 1346-1358 e1346, doi:10.1016/j.devcel.2021.04.006.
127. Feng, L.; Chao, J.; Zhang, M.; Pacquing, E.; Hu, W.; Shi, Y. Developing a human iPSC-derived three-dimensional myelin spheroid platform for modeling myelin diseases. *iScience* **2023**, *26*, 108037, doi:10.1016/j.isci.2023.108037.
128. Zeldich, E.; Rajkumar, S. Identity and Maturity of iPSC-Derived Oligodendrocytes in 2D and Organoid Systems. *Cells* **2024**, *13*, 674.
129. Ernst, R.J.; Krogager, T.P.; Maywood, E.S.; Zanchi, R.; Beranek, V.; Elliott, T.S.; Barry, N.P.; Hastings, M.H.; Chin, J.W. Genetic code expansion in the mouse brain. *Nat Chem Biol* **2016**, *12*, 776-778, doi:10.1038/nchembio.2160.
130. Guo, Q.R.; Cao, Y.J. Applications of genetic code expansion technology in eukaryotes. *Protein Cell* **2023**, 10.1093/procel/pwad051, doi:10.1093/procel/pwad051.

131. Meineke, B.; Heimgartner, J.; Eirich, J.; Landreh, M.; Elsasser, S.J. Site-Specific Incorporation of Two ncAAs for Two-Color Bioorthogonal Labeling and Crosslinking of Proteins on Live Mammalian Cells. *Cell Rep* **2020**, *31*, 107811, doi:10.1016/j.celrep.2020.107811.
132. Hao, M.; Ling, X.; Sun, Y.; Wang, X.; Li, W.; Chang, L.; Zeng, Z.; Shi, X.; Niu, M.; Chen, L.; Liu, T. Tracking endogenous proteins based on RNA editing-mediated genetic code expansion. *Nat Chem Biol* **2024**, 10.1038/s41589-023-01533-w, doi:10.1038/s41589-023-01533-w.
133. Kozma, E.; Kele, P. Bioorthogonal Reactions in Bioimaging. *Top Curr Chem (Cham)* **2024**, *382*, 7, doi:10.1007/s41061-024-00452-1.
134. Gow, A.; Devaux, J. A model of tight junction function in central nervous system myelinated axons. *Neuron Glia Biol* **2008**, *4*, 307-317, doi:10.1017/S1740925X09990391.
135. Gow, A.; Southwood, C.M.; Li, J.S.; Pariali, M.; Riordan, G.P.; Brodie, S.E.; Danias, J.; Bronstein, J.M.; Kachar, B.; Lazzarini, R.A. CNS myelin and Sertoli cell tight junction strands are absent in Osp/Claudin-11 null mice. *Cell* **1999**, *99*, 649-659.
136. Miyamoto, T.; Morita, K.; Takemoto, D.; Takeuchi, K.; Kitano, Y.; Miyakawa, T.; Nakayama, K.; Okamura, Y.; Sasaki, H.; Miyachi, Y., et al. Tight junctions in Schwann cells of peripheral myelinated axons: a lesson from claudin-19-deficient mice. *The Journal of Cell Biology* **2005**, *169*, 527-538.
137. Fannon, A.M.; Sherman, D.L.; Ilyina-Gragerova, G.; Brophy, P.J.; Friedrich, V.L., Jr.; Colman, D.R. Novel E-cadherin-mediated adhesion in peripheral nerve: Schwann cell architecture is stabilized by autotypic adherens junctions. *Journal of Cell Biology* **1995**, *129*, 189-202.
138. Eshed, Y.; Feinberg, K.; Poliak, S.; Sabanay, H.; Sarig-Nadir, O.; Spiegel, I.; Bermingham, J.R., Jr.; Peles, E. Gliomedin mediates Schwann cell-axon interaction and the molecular assembly of the nodes of Ranvier. *Neuron* **2005**, *47*, 215-229.
139. Stajkovic, N.; Liu, Y.; Arsic, A.; Meng, N.; Lyu, H.; Zhang, N.; Grimm, D.; Lerche, H.; Nikic-Spiegel, I. Direct fluorescent labeling of NF186 and NaV1.6 in living primary neurons using bioorthogonal click chemistry. *J Cell Sci* **2023**, *136*, doi:10.1242/jcs.260600.